



# E-Defense 2015 ten-story building: beam–column joint assessment according to different code-based design

C. Del Vecchio<sup>1</sup> · M. T. De Risi<sup>2</sup>  · C. Del Gaudio<sup>2</sup> · P. Ricci<sup>2</sup> · M. Di Ludovico<sup>2</sup> · Jae-do Kang<sup>3</sup>

Received: 31 May 2022 / Accepted: 24 January 2023  
© The Author(s) 2023

## Abstract

Recent devastating earthquakes worldwide pointed out the importance of seismic detailing and their influence on the observed damage and subsequent reparability of reinforced concrete buildings. Several studies and post-earthquake observations remarked the role of beam–column joints (BCJs) on the global building response and the effectiveness of transverse reinforcement in increasing the joint shear strength and the ultimate deformation. Although number of experimental and theoretical studies focused on the seismic response of BCJs, their mechanical behaviour is still a discussed topic. This resulted in number of design approaches available in worldwide code or standards that lead to different quantity of joint stirrups. This study focuses on the response of BCJs of a 10-story prototype building designed according to Japanese standards and tested in 2015 on the E-Defense shaking table. First the damage assessment at global (building) and local (joint) level is performed at increasing intensities and considering the building in the base slip and base fixed configurations. A refined numerical model is then developed and validated against global and local experimental results. Then, the joint stirrups are re-designed according to different international standards (ACI, EC8, NZS) and different numerical models are developed. The numerical results are then compared in terms of interstorey drift demand and joint shear strain. Finally, a comparison in terms of expected damage varying the design approach of joint stirrups is proposed.

**Keywords** Beam–column joints · Reinforced concrete · Non-linear · Numerical modelling · Damage states

---

✉ M. T. De Risi  
mariateresa.derisi@unina.it

<sup>1</sup> Department of Engineering, University of Sannio, Benevento, Italy

<sup>2</sup> Department of Structures for Engineering and Architecture, University of Naples Federico II, via Claudio 21, 80125 Naples, Italy

<sup>3</sup> National Research Institute for Earth Science and Disaster Resilience, Miki, Japan

## 1 Introduction

The seismic response of reinforced concrete (RC) buildings to large intensity earthquakes is often characterized by significant damage to structural and non-structural components (Kam et al. 2011; Ricci et al. 2011; Leon et al. 2012). This is commonly associated to significant economic losses and high repair costs (Di Ludovico et al. 2017; Del Vecchio et al. 2020) that may push the stakeholders to decide for the building demolition and reconstruction rather than a more expensive repair and retrofiting (Cuevas and Pampanin 2017; Bruneau and MacRae 2019). Post-earthquake inspections in the aftermath of recent devastating earthquakes (e.g. L'Aquila 2009, Christchurch 2011; Mexico 2017) showed that the shear cracking or brittle failure of under-designed RC members (e.g. short columns, beam–column joints, RC walls) may significantly compromise the building response resulting in the building collapse or unusability (Maeda and Kang 2009; Di Ludovico et al. 2017; Villalobos et al. 2018; Galvis et al. 2020; Lan et al. 2020; Yurdakul et al. 2021b). Often the damage is concentrated into beam–column joints with premature shear cracking related to the lack of a proper amount of transverse reinforcement (see Fig. 1) (Kam et al. 2011; Nagae et al. 2015).

Although the evolution of design codes led to the adoption of capacity design rules into design practice in the 70's (MOW 1976), minor attention was dedicated to the detailing of the joint panel. Indeed, the earthquakes in the 80's (El Asnam 1980; Mexico 1985; Loma Prieta 1989) resulted in a focus on these structural members. Before these events, although in some cases a minimum amount of joint shear reinforcement was used, the design of joint shear reinforcements was not directly considered in the codes or standards. This is because of the lack of widely accepted theories and formulations on the joint capacity, which resulted in a complete overlook in the design and construction practice (Paulay and Priestley 1992). The advancement in the scientific research pushed the adoption of design approaches of the into standard or pre-standard documents.



**Fig. 1** Damage to reinforced beam–column joints: Uto City Hall collapse in the 2016 Kumamoto earthquake (courtesy of Jae-do Kang) (a); due to the 2011 Christchurch earthquake (Leon et al. 2012) (b, c)

The first provisions in the United States standards appeared in ACI-ASCE 352 (1976) to limit the joint shear stresses in the joint panel. These limits were also adopted in ACI 318 (1995) where the nominal shear strength of the joint is proportional to the concrete compressive strength and depends on the joint type by using empirical values calibrated on experimental tests (Guimaraes et al. 1989). Furthermore, a minimum amount of transverse reinforcement is required. It can be assumed at least equal to the half of transverse reinforcements in the framing columns or other members which are expected to yield. The same approach is reported in the current ACI 318 (2011) with more details for minimum amount of internal stirrups and anchorage of longitudinal reinforcements. A similar approach to the American standards was adopted by the first version of the New Zealand standards NZS 3101 (1982). A substantial improvement in the New Zealand standards was achieved after the development of the strut and truss theory by Paulay and Priestley (1992). Replacing NZS 3101 (NZS 3101 1982), based on the diagonal stress limitation, NZS 3101 (1995) introduced novel formulations that allow to reduce the joint transverse reinforcements at least by 30% with respect to the previous code formulations (Park 1996). The same formulations are adopted by the current NZS 3101 (2006).

Japanese standards AIJ (1989) and following document until AIJ (2010) essentially focused on the diagonal concrete strut failure, assuming that sufficient joint shear reinforcements (minimum requirements are suggested) were provided in order to avoid other premature mechanisms.

In the European context, Eurocode 8 (EC8, CEN 2004) currently suggests two different design approaches for joint transverse reinforcement: limiting the principal tensile stress demand to avoid the joint cracking; preserving the joint panel integrity in the post-cracking stage based on the strut and truss theory mentioned above (Pauley and Priestley 1992; Fardis 2009) similarly to NZS 3101 (2006). The current Italian building code (D.M. 2018) and its previous version (D.M. 2008) implemented the same design principles of the EC8 for joints, thus substituting the previous Ministerial Decree (D.M. 1996, Circolare 1997). The latter suggested, for the first time in Italy, the use of joint stirrups extending those of the bottom column into the joint panel. It is worth mentioning that the current D.M. 2018-based design often leads to a high number of joint stirrups that makes difficult their installation within the joint panel. This commonly force the designers to use high column cross-sections.

Thus, because the evolution of seismic codes worldwide had significant time differences country-by-country and because of the absence of a unified approach to design joint stirrups, it is notable that many structural systems are vulnerable to seismic events because of the lack of proper amount of transverse reinforcement in the joint panel. This may lead to the cracking of the joint panel before the full development of the ductility of the framing members often concentrating the inelastic demand in the joint region (Hakuto et al. 2000; Nagae et al. 2015; Shiohara 2017). Because the joint nonlinear response is mainly governed by a shear mechanism, the prediction of the ultimate capacity and the joint reparability after significant cracking are critical issues. This makes the experimental and analytical studies on the influence of joint response on the seismic performance of RC buildings of paramount importance. Many research studies focused on these topics in the recent years proposing relevant analytical models (Shiohara and June 1998; Favvata et al. 2008; Kim and LaFave 2012; Jeon et al. 2014; Favvata and Karayannis 2014) that were also implemented in useful software tools (e.g. ADAPTIC, Izzuddin 2009). Other studies proposed fragility curves to quantify the damage (Pagni and Lowes 2006; Brown and Lowes 2007; Lowes and Li 2009) and assess the joint reparability (Yurdakul et al. 2021a).

In this context, a unique experimental program was conducted by using the E-Defense shaking table (Tosauchi et al. 2017; Kajiwara et al. 2021) on full-scale 10-storey RC buildings relying on shear walls ( $x$  direction) and moment resisting frames ( $y$  direction) designed according to AIJ standard (AIJ 2010). The experimental program had the main scope to assess the influence

of novel sliding and uplifting base surface to contain the earthquake damage and to assess the damage evolution and residual capacity on a classic fixed-base structure (Kajiwara et al. 2021).

This study focuses on the nonlinear response of beam–column joints belonging to the frames in the  $y$  direction. First the experimental results of the 2015 test in terms of global and local (at joint level) response are analysed. The joint shear distortion as well as the interstorey drift demand are used to quantify the damage states and assess the influence of the joint on the global building response. A 3D refined numerical model is implemented to reproduce the building local and global response. This model is later used to quantify the influence of the joint stirrups design procedure according to different international standards on the joint response and predicted earthquake damage.

## 2 Influence of BCJ in the E-Defense 2015 test

The 10-storey full-scale RC building tested in the 2015 is 27.45 m height and has in-plane dimensions of 12.0 m and 8.0 m measured at the centreline of base columns. It relies on moment resisting frames (MRFs) in the  $y$  direction and dual systems (shear wall + MRF) in the  $x$  direction. The weight of each storey is about 80 tons, and the total weight of the specimen, including the basement, is about 1000 tons. The structural system was designed according to AIJ (2010) considering capacity design rules. In turn, column-to-beam moment capacity ratio higher than one is assumed at all floors to guarantee a beam sidesway mechanism (Tosauchi et al. 2017). The beam–column joints were designed considering a ratio of shear force over shear strength acting on beam–column joints equal to 1.0 or below for all beam–column joints. The minimum shear reinforcement ratio (i.e. 0.2%) suggested by the code was used for all the joints. Since the main focus of this paper is the response of BCJs in MRFs, only the response of the building in the  $y$  (frame) direction—where joints resulted more damaged, as described below—is considered. An overview of the building and structural details of reference joints is reported in Fig. 2 and a summary of the main properties of BCJ in the frame direction is shown in Table 1. More

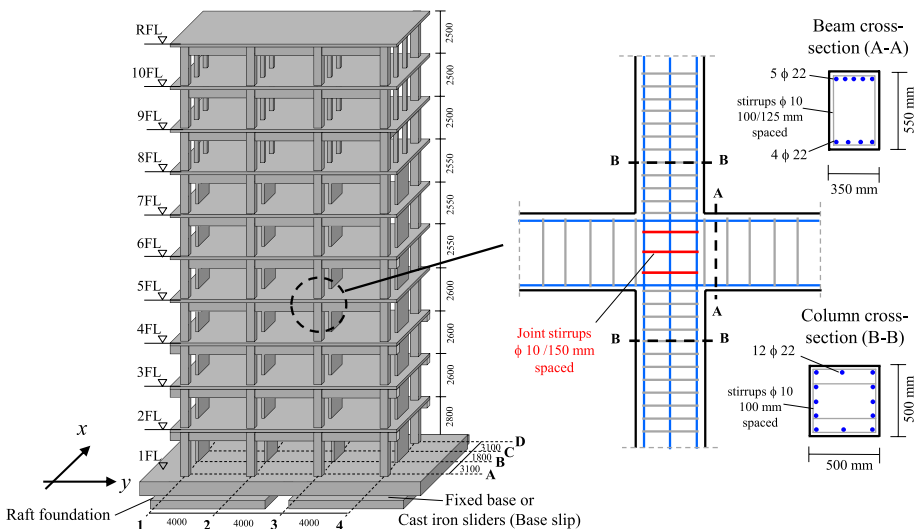


Fig. 2 Overview of the building geometry and reinforcement details of reference joints

**Table 1** Geometry and reinforcement details of the structural members in the Frame direction (y)

Floor	Joint	Type	Transv. beams	b <sub>c</sub> (mm)	h <sub>c</sub> (mm)	φ <sub>s,l,b</sub> (mm)	N <sub>s,l,b</sub> <sup>top</sup> (-)	N <sub>s,l,b</sub> <sup>bot</sup> (-)	b <sub>b</sub> (mm)	h <sub>b</sub> (mm)	f <sub>c</sub> (MPa)	f <sub>yl</sub> (MPa)	f <sub>yw</sub> (MPa)
2FL	A1, A4, D1, D4	Ext	1	550	550	22	6	5	350	550	68.7	396	387
	A2, A3, D2, D3	Int	1	550	550	22	5	4	350	550	68.7	396	387
3FL	A1, A4, D1, D4	Ext	1	550	500	22	6	5	350	550	72.0	366	387
	A2, A3, D2, D3	Int	1	550	500	22	5	4	350	550	72.0	366	387
4FL	A1, A4, D1, D4	Ext	1	500	500	22	5	5	350	550	57.6	397	387
	A2, A3, D2, D3	Int	1	500	500	22	5	4	350	550	57.6	397	387
5FL	A1, A4, D1, D4	Ext	1	500	500	22	5	4	350	550	47.7	387	387
	A2, A3, D2, D3	Int	1	500	500	22	4	4	350	550	47.7	387	387
6FL	A1, A4, D1, D4	Ext	1	500	500	22	5	4	350	550	45.5	392	387
	A2, A3, D2, D3	Int	1	500	500	22	5	3	350	550	45.5	392	387
7FL	A1, A4, D1, D4	Ext	1	500	500	22	4	4	350	550	53.0	392	387
	A2, A3, D2, D3	Int	1	500	500	22	4	3	350	550	53.0	392	387
8FL	A1, A4, D1, D4	Ext	1	500	500	19	5	4	350	550	49.0	380	387
	A2, A3, D2, D3	Int	1	500	500	19	4	3	350	550	49.0	380	387
9FL	A1, A4, D1, D4	Ext	1	500	500	19	4	3	350	550	51.9	397	387
	A2, A3, D2, D3	Int	1	500	500	19	4	3	350	550	51.9	397	387
10FL	B1, B4, C1, C4	Ext	2	500	230	19	3	3	350	550	51.9	397	387
	B2, B3, C2, C3	Int	2	500	230	19	3	3	350	550	51.9	397	387
	A1, A4, D1, D4	Ext	1	500	500	19	4	3	300	500	43.9	401	387
	A2, A3, D2, D3	Int	1	500	500	19	3	3	300	500	43.9	401	387
	B1, B4, C1, C4	Ext	2	500	230	19	3	3	300	500	43.9	401	387
	B2, B3, C2, C3	Int	2	500	230	19	3	3	300	500	43.9	401	387

**Table 1** (continued)

Floor	Joint	Type	Transv. beams	$b_c$ (mm)	$h_c$ (mm)	$\phi_{s,l,b}$ (mm)	$N_{s,l,b}^{top}$ (-)	$N_{s,l,b}^{bot}$ (-)	$b_b$ (mm)	$h_b$ (mm)	$f'_c$ (MPa)	$f_{y,l}$ (MPa)	$f_{y,w}$ (MPa)
RFL	A1, A4, D1, D4	Ext	1	500	500	19	3	3	300	500	41.0	392	387
	A2, A3, D2, D3	Int	1	500	500	19	3	3	300	500	41.0	392	387
	B1, B4, C1, C4	Ext	2	500	230	19	3	3	300	500	41.0	392	387
	B2, B3, C2, C3	Int	2	500	230	19	3	3	300	500	41.0	392	387

Ext. and Int. refers to the joint type (exterior or interior);  $b_c$  is the column width;  $h_c$  is the column height;  $\phi_{s,l,b}$  is the diameter of longitudinal reinforcements;  $N_{s,l,b}^{top}$  is the number of beam longitudinal top reinforcement;  $N_{s,l,b}^{bot}$  is the number of beam longitudinal bottom reinforcement;  $b_b$  is the beam width;  $h_b$  is the beam height;  $f'_c$  is the mean concrete compressive strength;  $f_{y,l}$  is the mean yielding strength of longitudinal reinforcement;  $f_{y,w}$  is the mean yielding strength of transverse reinforcement

details on the building design can be found in Kajiwara et al. (2021), while details on the adopted numerical model are reported in Di Domenico et al. (2023).

## 2.1 Main experimental results in E-Defense 2015 test

A series of shaking table tests increasing the earthquake intensity were performed on the same prototype building tested first in the base slip (BS) and then in base fixed (BF) configuration. They were subject to increasing intensities of 10%, 25%, 50% and 100% of the Kobe earthquake (JMA-Kobe) corresponding to a peak ground acceleration recorded on the table of about 0.08 g, 0.20 g, 0.35 g and 0.75 g, respectively. Before the BS test, the measured fundamental period of vibration was equal to 0.57 s, both in the (x) wall and in the (y) frame direction.

The main experimental outcomes of the tests performed at E-Defense in 2015 were described in detail in Kajiwara et al. (2021), Kajiwara et al. (2017), Sato et al. (2017), Tosauchi et al. (2017). They clearly highlighted a key role of damage in beam–column joints especially for the fixed-based building configuration (Fig. 3). As a matter of fact, observed damage during the Base-Slip test was not significant. It mainly consisted of cracks at the beams ends that were generally lower than 0.05 mm wide. Slight cracks were observed in some of the BCJs between ground and sixth floor. Furthermore, it was observed that all reinforcement bars were maintained in the elastic region and the maximum inter-story drift ratio achieved during the run to 100% of the reference earthquake slightly exceeded the 0.5%. The latter is commonly considered in international standards (CEN 2004; AIJ 2010) as the threshold for damage limitation in RC frame structures. This proved the effectiveness of the adopted base-isolation system to preserve the building from significant damage.

Before the beginning of tests on the BF configuration (i.e., with the specimen fully fixed to the shaking table after completing the test in the BS configuration), the measured fundamental periods of vibration were equal to 0.58 s and 0.85 s, in the (x) wall and in the (y) frame direction, respectively. This pointed out the (expected) stiffness decrease associated with the damage observed at the end of the BS test. Then, during the BF test under 50% of the reference earthquake, cracks at beams ends and in the joint panels were up to around 0.15 mm wide. For increasing seismic intensity to 100% of the Kobe earthquake, the damage in beam–column joints progressed further until the concrete cover spalling with joint hoops partly exposed. Cover spalling was also observed on the base columns and on the shear wall. The damage to BCJs was classified as level III or IV (moderate or heavy) according to the AIJ- Post-Earthquake Temporary Risk Evaluation of Damaged Buildings damage classification (JBDPA 2015). Figure 2 shows the final damage state after 100%-Kobe input

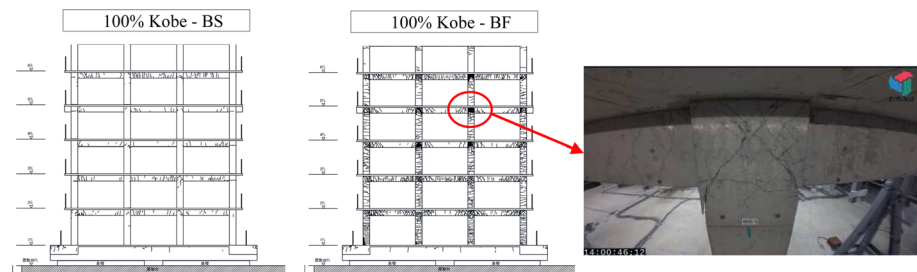
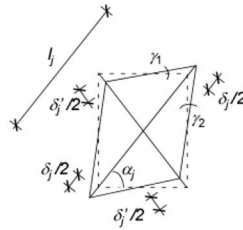
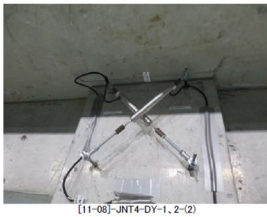


**Fig. 3** Main damages in frame direction after fixed-based test—interior joint at fourth floor



$$\gamma_j = \frac{\delta_j - \delta'_j}{2l_j} \left( \tan \alpha_j + \frac{1}{\tan \alpha_j} \right)$$

Fig. 4 Calculation of the experimental joint shear strains

for the Base-Slip and the Base-Fixed building in the frame direction. It can be noted that damage is concentrated from the first to the sixth floor, especially in beam–column joints. It is worth nothing that the foundation reported vertical cracks at the top side of the two end-ing portions. They were related to the lifting of the specimen with the crane.

Since some interior joints in the frame direction were monitored during the tests by means of two diagonal Linear Variable Displacement Transducers (LVDTs) each, joint shear strains ( $\gamma_j$ ) can be computed from LVDT deformations ( $\delta_j$ ) for each seismic intensity (or, equivalently, for each scale factor, SF) and both the tested configurations, as shown in Fig. 4. Resulting maximum values of joint shear strain values ( $\gamma_{j,max}$ ) for each scale factor are reported in Fig. 5. It can be noted that maximum joint strains were achieved always between the third and sixth floor, where, for the Base-Slip building,  $\gamma_{j,max}$  ranged from about 0.1% to 0.2% at 50% Kobe, and from 0.25% to 0.32% at 100% Kobe. In the BF configuration joint shear strains significantly higher than BS were achieved. The maximum recorded joint shear strain,  $\gamma_{j,max}$ , at 100% Kobe is about 1.8%.

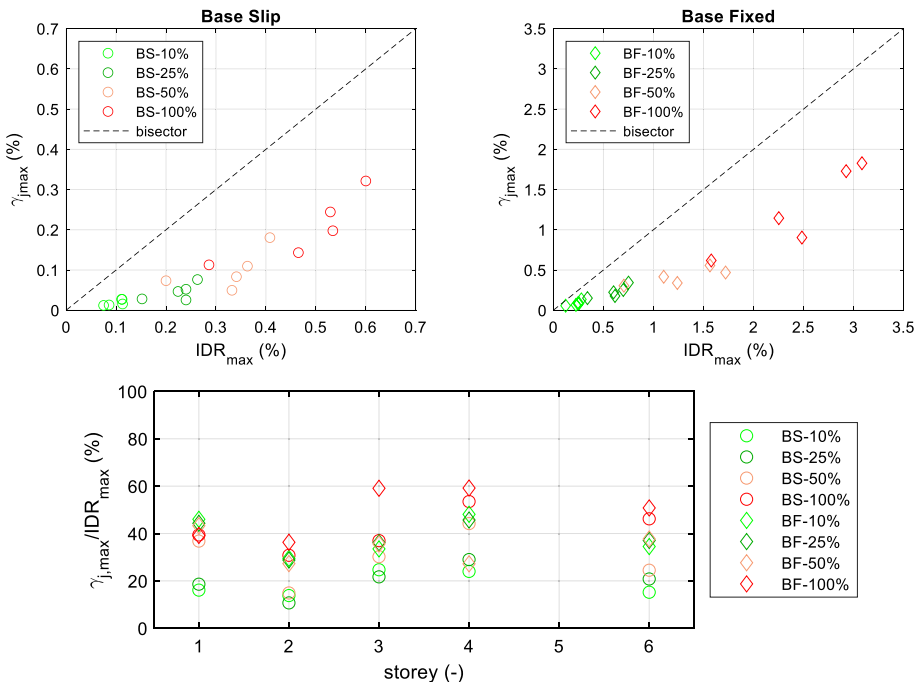
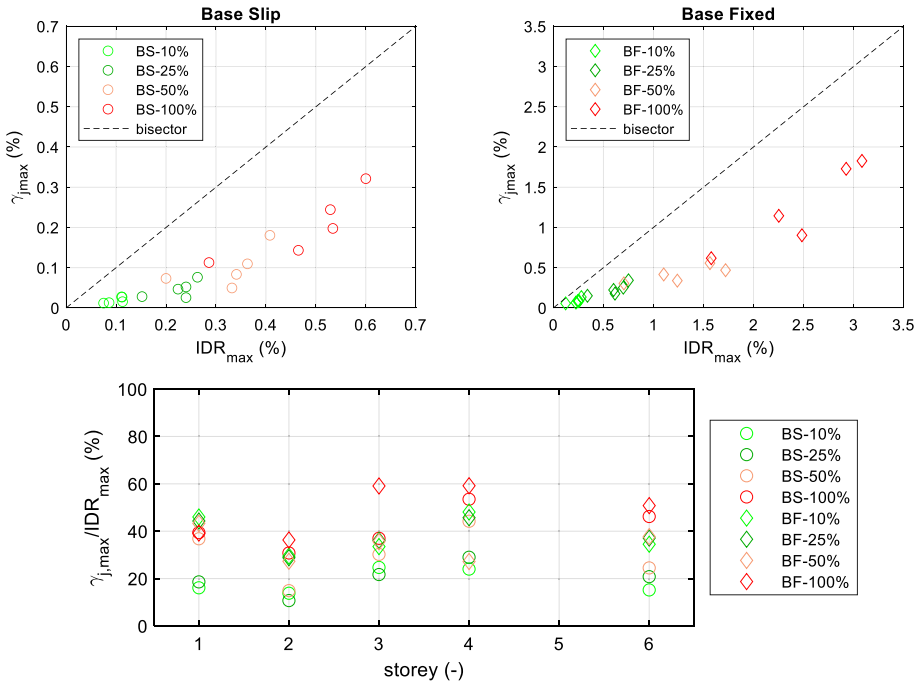


Fig. 5 Experimental maximum joint shear strains for the (interior) monitored joints





**Fig. 6** Experimental values of  $\gamma_{j,max}$  versus  $IDR_{max}$  and  $\gamma_{j,max}/IDR_{max}$  ratios for the (interior) monitored joints–frame direction

Another clear proof of the key role played by beam–column joints in these tests is provided by the percentage weight of  $\gamma_{j,max}$  on the maximum Interstorey Drift Ratio (IDR), as shown in Fig. 6. Obviously, the IDR experienced at a given story depends on the rotational (mainly flexural in this case) contribution of beams and columns at that story and on the joint shear deformability contribution. Therefore, the role of joints can be quantified by means of the ratio between  $\gamma_{j,max}$  and  $IDR_{max}$  at each story measured in the same (frame) direction. Figure 6 shows that, for the Base-Slip test, at 100% Kobe,  $\gamma_{j,max}$  reaches the 54% of the maximum IDR (at the fourth floor). Similarly, for the fixed-based building, at the maximum seismic intensity,  $\gamma_{j,max}/IDR_{max}$  is about 60% (at the same floor).

## 2.2 Experimental damage to BCJ in E-Defense 2015 test

To further discuss on the role of BCJs on the building response, the experimental local (joint) and global damage are analyzed in this section. To this end, damage measures at the building and joint panel level are needed. Different classifications are available in literature (Pagni and Lowes 2006; Brown and Lowes 2007; Lowes and Li 2009; Cardone 2016). They were calibrated on different dataset of experimental tests on BCJs designed according to different design principles and, thus, having different geometry and reinforcement details.

In this study, the damage states (DSs), damage descriptions and the fragility functions proposed in the FEMA P-58/BD-3.8.6 (Lowes and Li 2009) for RC frame sub-assemblages (i.e. ensemble of columns, beams and joint panel) are used. Experimental data for six RC frame categories, characterized by different design levels available in the US standards

**Table 2** Definition of damage states (DSs)

Damage state	Damage description	Repair action	IDR (%) for OMF -BYJF (Lowes and Li, 2009)		Joint shear strain (%) (Brown and Lowes, 2007)	
			Mean	St.dev.	Mean	St.dev.
DSC	Hairline cracking	Cosmetic repair	0.42	0.18	0.42	0.26
DS0	Joint/beam/column crack width > 0.5 mm (long/transv. Reinforcement yielding)	Epoxy injection	1.19	1.01	0.74	0.49
DS1	Joint crack width >1.3 mm beam/column crack width >1.5 mm	Epoxy injection	1.75	0.35	n.a.	n.a.
DS2	Spalling of concrete in the joint >10%, spalling of concrete cover in beams and columns	Patch concrete	2.15	0.47	3.79	1.40
DS3	Spalling of concrete in the joint >80%, concrete crushing	Replace concrete	3.18	0.86	n.a.	n.a.
DS4	Buckling of column longitudinal reinforcement	Replace reinforcing steel/Replace joint	5.00	0.95	n.a.	n.a.

for RC members, are available in Lowes and Li (2009). They are: ACI Special Moment Frames (SMF); ASCE Category 1 Frames (ASCE1); ACI Intermediate Moment Frames (IMF); ASCE Category 2 Frames (ASCE2); ACI Ordinary Moment Frames Controlled by Beam Yielding or Joint Failure (OMF-BYJF); ACI Non-Compliant Frames (NCF/ASCE3). Since the BCJs of the tested building were designed according to non-US standards, it is not easy to find a direct correlation with one of these categories. In this study, the category OMF-BYJF is selected since it contains the highest percentage of specimens with a failure mode similar to that observed on the BCJs of the building prototype (i.e. beam-yielding combined with a significant joint cracking). Furthermore, within the three categories having a similar failure mode (i.e. IMF, ASCE2 and OMF-BYJF), this is the category with the mean joint transverse steel ratio closest to the 0.2% used in the building prototype.

The DSs, the description of damage, the related repair actions, the mean drift and the standard deviation (St.dev.) estimated from the experimental database are reported in Table 2, along with the mean values and standard deviations of joint shear strain at each DS as suggested by Brown and Lowes (2007). An overview of the damage on the joint panel is reported in Fig. 7 with reference to a joint subassembly tested by Lehman et al. (2004). It is worth mentioning that joint shear strain-based damage scale refers to a different dataset of BCJs (Brown and Lowes 2007) including tests on joints belonging to different categories. This is because experimental data on joint shear strain were not often recorder or reported in literature and limited data are available.

The DSC refers to slight damage where hairline crackssing (see Fig. 7a) is expected and a cosmetic repair consisting in the replacement and repair of finishes is suggested. The joint cracking with crack width >0.5 mm is expected at DS0 along with the yielding of longitudinal and transverse reinforcement. Crack width > 1.3 mm is expected at DS1 (see Fig. 7b). Epoxy injection with replacement of finishes is suggested at DS0 and DS1. The

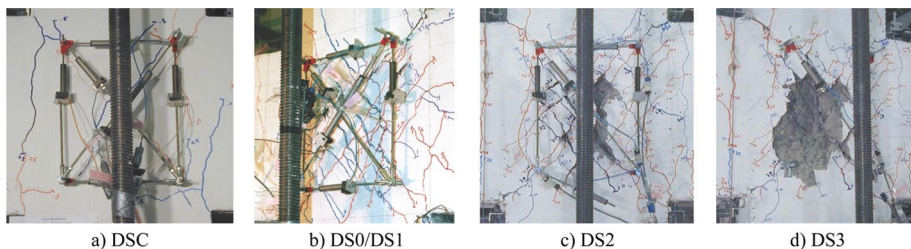
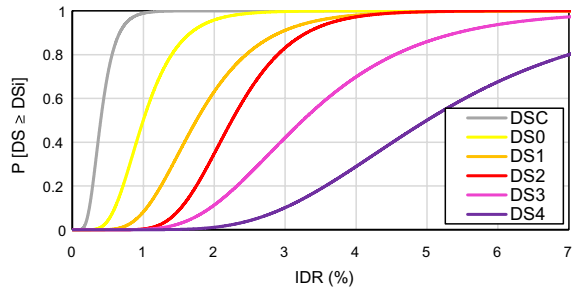


**Fig. 7** Typical damage to RC frame sub-assemblage for each DS (Lehman et al. 2004): DSC (a); DS0/DS1 (b); DS2 (c); DS3 (d)

**Table 3** Main parameters of the adopted fragility curves for damage analysis

Damage State	IDR-based fragility curves used herein	
	$\theta$ (%)	$\beta$
DSC	0.40	0.40
DS0	1.00	0.40
DS1	1.75	0.40
DS2	2.25	0.30
DS3	3.25	0.40
DS4	5.00	0.40



DS2 is characterized by significant damage to the joint panel with concrete spalling on a surface area > 10% (see Fig. 7c). Patching of damaged concrete is suggested in addition to the repair actions suggested in the lower DSs. It is worth noting that the repair costs associated to these repair actions may exceed the 50% of the cost of demolition and reconstruction of the entire joint subassembly, thus making the repair not convenient (Applied Technology Council 2012). The DS3 reflect a severe damage of the joint panel with spalling on most of the panel area and crushing of concrete (Fig. 7d). Although replacement of concrete is suggested as typical repair action, the repairing could be not sustainable from the economic standpoint. The DS4 is characterized by the collapse of the joint subassembly with buckling of column longitudinal reinforcement passing through the joint. Typically, the joints that achieved this DS have limited residual capacity to sustain seismic actions.

Starting from empirical data reported in Table 2, Lowes and Li (2009) proposed three fragility curves in terms of maximum achieved IDR for DS1, DS2 and DS3, as lognormal functions characterised by the logarithmic means and logarithmic standard deviations shown in Table 3. Herein, such fragility curves are adopted, and integrated, for the purposes of this work, with two further curves at DSC and DS0. Thus, the latter are defined, similarly to what suggested for DS1–DS3 by Lowes and Li (2009), as lognormal fragility curves characterised by a logarithmic mean equal to median values of data collected by Lowes and Li (2009) for OMF-BYJF joints at DSC and DS0, and a logarithmic standard deviation equal to the highest value suggested for the DS1–DS3 by Lowes and Li (2009) (i.e., 0.40). Assumptions similar to DSC and DS0 are advanced herein for DS4 (which, however, is generally not involved at all in the following damage analyses). A summary of the main parameters (mean drift,  $\theta$  and standard deviation,  $\beta$ ) for the adopted IDR-based fragility curves is shown in Table 3 along with a graphical representation of the curves.

Therefore, the DS achieved at each floor under the selected earthquake intensity is attributed to the building in the BS and BF configurations based on the probability of occurrence of each DS, estimated by means of the fragility curves defined above. For each test, the probability of occurrence of each DS can be defined at each storey, given the experimental value of  $IDR_{max}$  recorded at that storey during the test. The DS with the maximum probability of occurring at each floor is herein defined as  $DS_{Pmax}$ .

The prototype building in the base-slip configuration showed low-sensibility to damage at moderate and high intensity earthquakes. Indeed, based on the distribution of  $IDR_{max}$  along the height, the DS experienced in the frame direction under 25% and 50% of the Kobe earthquake can be classified as Null and a few (intermediate) stories reach  $DS_{Pmax}$ =DSC. Under 100% of the earthquake intensity (Fig. 8a), the  $DS_{Pmax}$  is still DSC at almost all floors, but the  $IDR_{max}$  of 4th floor is closer to the lower bound (16th percentile) of the DS0 and larger cracks are expected. In turn, at 100% Kobe, the building

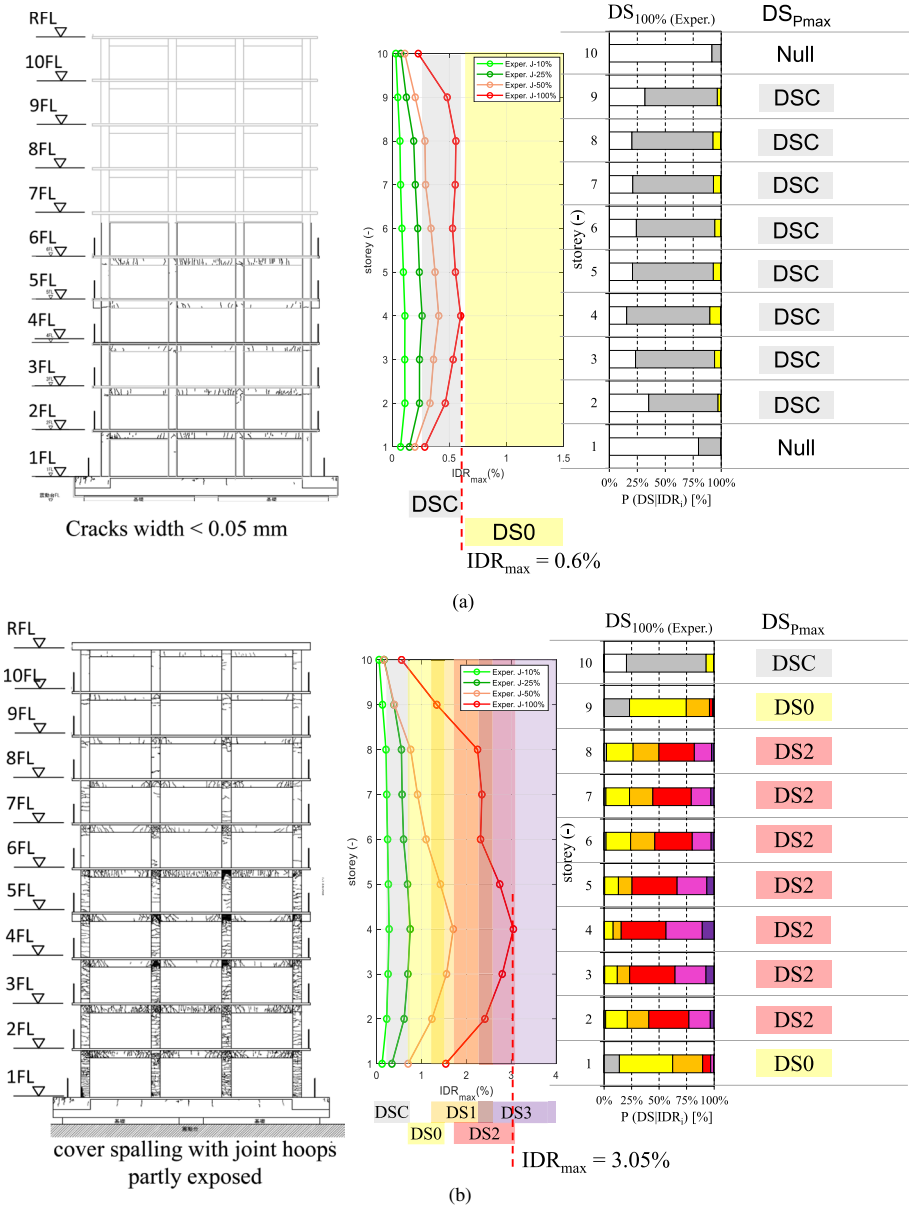


**Fig. 8** Achieved DS during the 2015 test in the base-slip (a) and base-fixed (b) configurations. Colour strips in IDR<sub>max</sub> distribution plot indicated the 16th–84th percentiles ranges

in the BS configuration mostly experienced a DS = DSC. The attributed DSs well reflect the experimental observations. Indeed, as reported in Kajiwara et al. (2021), hairline cracking to structural members with crack width lower than 0.05 mm were observed (see Fig. 8a). The IDR<sub>max</sub> for 100% intensity is about 0.6% slightly higher than the limit of 1/200 according to allowable stress design principles (CEN 2004; AIJ 2010). Furthermore, all reinforcements experienced an elastic response. This confirmed that structural members do not need

specific repair actions and only cosmetic repair of plaster and finishes could be needed, along with the effectiveness of the proposed base slip solution to contain the damage under severe earthquake loads.

Figure 8b reports the damage classification in terms of  $DS_{P_{max}}$  of the prototype building tested in the fixed-base configuration at 100% Kobe. Before considering the maximum seismic shaking, by using the  $IDR_{max}$  based classification, the buildings experienced a DS Null and  $DS=DSC$  under the 10% and 25% of the Kobe earthquake at most of the floors, respectively. By increasing the earthquake intensity to 50%, intermediate floors (from 2nd to 6th) showed a drift demand significantly higher than other floors, showing  $DS_{P_{max}}=DS0$ . The test to 100% of the earthquake intensity confirmed the damage localization at intermediate floors with a peak  $IDR_{max}$  at the 4th floor of about 3.05%. By using the drift-based damage classification, the intermediate floors (3rd to 5th) experienced a  $DS_{P_{max}}$  that can be DS2 or DS3 with very similar probability, thus confirming the moderate to heavy damage attributed to BCJs according to the AIJ damage classification (Tosauchi et al. 2017). Under the intensity of 100% Kobe, most of the floors exhibited a  $DS_{P_{max}}=DS2$ , thus with spalling of concrete cover on the main structural members. Patching or replacement of damaged concrete is suggested as main repair action. However, the cost of these activities may exceed the 50% of the cost related to demolition and reconstruction, thus making not convenient the repair.

Even though a good agreement was found between the damage description related to the adopted IDR-based damage analysis and the experimental one, the same matching is not found in terms of the local damage at level of the BCJs, if damage classification proposed by Brown and Lowes (2007) in terms of  $\gamma_{j,max}$  is adopted. First, it can be noted that any information is provided for joint shear strain thresholds at DS1 and DS3, due to a lack of experimental data. Then, comparing the ranges of  $\gamma_{j,DSi}$  shown in Table 2 with  $\gamma_{j,max}$  obtained experimentally (Fig. 6), it can be concluded that, the maximum damage achieved under 100% Kobe earthquake for the BF-test would be classified in the range DS0-DS1 (i.e., joint cracking > 1.3 mm). This does not match with the description of the experimental damage on the joint panels of the 4th floor where a partly spalling of concrete cover was detected. Therefore, if the damage analysis is performed considering the joint shear strain,  $\gamma_{j,max}$ , an underestimation of the observed damage is found. A possible explanation of such a difference can be found analysing the dataset of experimental tests used to calculate the joint shear strain-based DSs. Indeed, the dataset used by Brown and Lowes (2007) contains tests on BCJ subassembly with a transverse steel ratio in the joint panel higher than that used in the joints of the prototype building or of the joints considered in the OMF-BYJF category considered to calculate IDR-based DSs. Therefore, only the  $IDR_{max}$ -based classification is actually applied hereinafter.

### 3 Design of BCJs according to different code prescriptions

BCJs in the investigated prototype building tested in 2015 at E-Defense were designed according to AIJ (2010) standards. Several other modern codes worldwide consider specific provisions in the definition of beam–column geometric dimensions and of the reinforcement amount in the design of beam–column joints of RC buildings. Despite the object of these provisions (beam–column joint) and the considered load typology (gravity and seismic actions) are the same worldwide, existing code prescriptions can be quite different from country to country, e.g. for what concerns: (1) the computation of the joint strength, (2) the calculation of the horizontal/vertical reinforcement amount, (3) the effect of biaxial loadings on the evaluation of joint strength.

**Table 4** Main features of code-based models used worldwide

	EC8 (2004)	NZS-3101-1 (2006)	ACI 318 (2019)	AIJ (2010)
Shear strength mechanisms	Truss + Strut	Truss + Strut	Strut	Strut
Diagonal compressive strut check	$V_{jh} \leq \eta f_c \sqrt{1 - \frac{v}{\eta} b_j h_c}$	$V_{jh} \leq \min(0.2f_c b_j h_c; 10b_j h_c)$	$V_{jh} \leq \alpha \lambda \sqrt{f_c} A_{jh}$	$V_{jh} \leq k_A (f_s - 0.5) b_j D$
Horizontal stirrups	<p><i>Pre-cracking approach (EC8-1)</i></p> $\frac{A_{sh} f_{yw}}{b_j h_{yw}} \geq \frac{\left(\frac{v_{jh}}{s_{yw}}\right)^2}{f_c + v f_c} - f_{ct}$ <p><i>Post-cracking approach (EC8-2)</i></p> <p>Exterior Joints:  <math>A_{sh} f_{yw} \geq A_{s2} f_c (1 - 0.8v)</math></p> <p>Interior Joints:  <math>A_{sh} f_{yw} \geq (A_{s1} + A_{s2}) f_c (1 - 0.8v)</math></p>	<p>Exterior Joints:  <math>A_{sh} = \frac{6V_{jh} \beta f_c A_c}{f_c A_c} \frac{f_{yw}}{f_{yw}} \left(0.7 - \frac{C_j N}{f_c A_{jh}}\right)</math></p> <p>Interior Joints:  <math>A_{sh} = \frac{6V_{jh}}{f_c A_{jh}} \cdot \frac{\alpha f_c A_c}{f_{yw}}</math></p>	$\rho_{jh} = \begin{cases} 0.3 \left( \frac{A_{sh}}{A_{jh}} - 1 \right) \frac{f_c}{f_{yw}} \\ 0.09 \frac{f_c}{f_{yw}} \\ 0.2 k_f k_{m1} \frac{f_{yw} N}{f_{yw} A_{jh}} \end{cases}$	$\rho_{jh} = \frac{A_{sh}}{b_s}$
Vertical Reinforcement	<p>Not considered</p>	<p>Not considered</p>	Not considered	Not considered
Biaxial loading	<p>Not considered</p>	$A_{sv} = \alpha_v A_{sh} \frac{f_{yw}}{f_y} \frac{h_b}{h_c}$ $C_j = \frac{V_{jh}}{V_{jh} + V_{jx}}$	Not considered	Not considered

$A_{ch}$  = column area within the concrete cover;  $A_g$  = column gross area;  $A_{jh}$  = joint horizontal area;  $A_{s1}$ ,  $A_{s2}$  = upper and lower longitudinal reinforcement in the adjacent beam;  $A_{sh}$  = joint stirrups area;  $b$  = column base;  $b_j$  = joint base;  $f_c$  = concrete compressive strength;  $f_{ct}$  = concrete tensile strength;  $f_y$  = yielding stress of longitudinal reinforcement;  $f_{yv}$  = yielding stress of vertical reinforcement in the joint panel;  $f_{yw}$  = yielding stress of joint stirrups;  $h_b$  = beam height;  $h_c$  = column height;  $h_{pw}$  = joint vertical height;  $k_f$  = concrete strength factor;  $k_{m1}$  = confinement strength factor;  $N$  = column axial load;  $s$  = stirrups spacing;  $V_{jh}$  = horizontal joint shear demand;  $V_{jx}$  = joint shear demand in x-direction;  $V_{jy}$  = joint shear demand in y-direction;  $\alpha_v$  = coefficient depending on the column axial load;  $\eta$ ,  $\alpha$ ,  $\lambda$ ,  $k_A$ ,  $\beta$  = joint typology coefficients;  $v$  = column axial load ratio

In this work, the current versions of the European (EC8-part 1, CEN 2004), American (ACI 318 2019) and New Zealand (NZS, 3101-part 1 2006) standards for design are considered, along with the Japanese code used for the design of 2015 tests (AIJ 2010)—see Table 4.

Despite of some minor differences in safety factors or for the consideration of reinforcing steel hardening, all codes agree in defining joint shear demand as a function of the maximum tensile action coming from the yielding of the adjacent beams, in agreement with (worldwide adopted) capacity design principles.

The first main difference among codes is about the shear mechanisms they consider in the design formulation depending on the different literature studies.

EC8-part 1 (CEN 2004) and NZS, 3101-part 1 (2006) assume the co-existence of strut and truss resisting mechanisms for reinforced joints, leading to (1) the definition of geometric joint dimensions necessary to not overcome the diagonal strut compressive strength, and (2) the calculation of the number of horizontal stirrups and vertical reinforcement in joints to resist to the portion of shear load that diagonal compressive strut is not able to absorb (Paulay and Priestley (1992); Fardis 2009). It is worth noting that an alternative approach for reinforcement design is also allowed by EC8 (EC8-1 in what follows, see Table 4). The latter (EC8-1 in what follows) can be used equivalently to the previously mentioned one (EC8-2), and it assumes that stirrups in joints in pre-cracking condition can offer a beneficial confining effect on the diagonal resisting compressive strut that prevent joint cracking. EC8-1 and EC8-2 often lead to quite different amount of transverse reinforcement (as demonstrated later for the case-study building).

On the other hand, AIJ (2010) and ACI 318 (2019) only prescribe the safety check of the compressed diagonal strut (or, equivalently, the definition of the joint resisting area). According to ACI 318 (2019), joint stirrups are designed to match the minimum requirements in terms of geometrical percentage (prescriptions related to Special Moment Resisting Frames are used in what follows). As a matter of fact, commentary to ACI 318 (2019), based on ACI 352R, explicitly allows neglecting the contribution of joint stirrups based on the experimental evidence (Meinheit and Jirsa 1977) that transverse reinforcement didn't provide any beneficial effect on the joint strength if a minimum stirrups amount is provided. However, the minimum amount of transverse reinforcement required by the ACI 318 is generally very high as shown later and significantly higher than that prescribed by AIJ (only 0.2%—AIJ 2010). Recent research works (e.g. Shiohara and Kusahara 2014) contributed to this topic with the scope to update the design of joint transverse reinforcement in Japanese standards.

Among the codes analyzed herein, the effect of biaxial loading on joint shear strength is explicitly considered only by NZS-3101, based on Pauley and Priestley (1992)'s recommendations, by means of a factor ( $C_j$ ), which proportionally allocates the beneficial effect of axial compression load to the two loading directions of the lateral design forces under biaxial loading.

As a result of the application of the above-mentioned codes, Fig. 9 reports the minimum required geometric percentage of transverse reinforcement ( $\rho_{jh}$ ) for exterior and interior joints in the frame direction. It is worth mentioning that mean value of mechanical properties (both for concrete and reinforcing steel) and gravity axial load ratio are used for this calculation. With reference to EC8, the highest number of stirrups is always provided by EC8-2 approach. Since approach EC8-1 and EC8-2 can be alternatively used, the minimum  $\rho_{jh}$  is assumed herein as representative of EC8-compliant design (namely, always the EC8-1 approach). Looking at EC8-1 approach,  $\rho_{jh}$  increases if  $f_c$  decreases or when the longitudinal amount of beam reinforcement increases (as expected due to the increase of joint shear



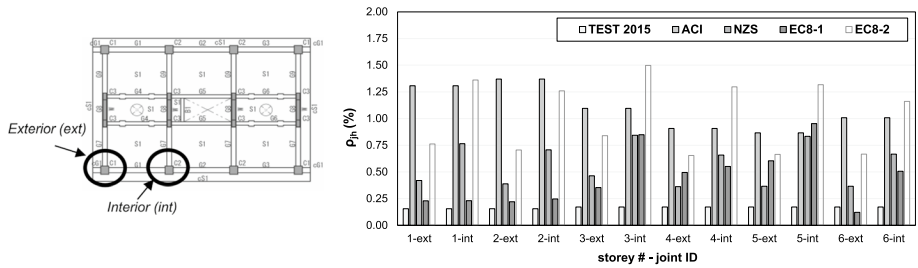


**Fig. 9** Geometric percentage of stirrups designed according to different codes for interior and exterior joints of 2015-E-Defense tests—1st to 6th floor, frame direction (“TEST 2015” was designed according to the AIJ code)

demand in this case). It can be also noted that the highest amount of stirrups percentage is necessary from the 3rd to the 6th floor (namely, the floors where joints were highly damaged in 2015-test, as commented in Sect. 2). Lastly, it is worth noting that the highest amount of required stirrups percentage is (almost always) obtained if ACI-318 prescriptions are applied (despite it represents just a “minimum amount” according to that code).

It should be noted that modern seismic codes, like those investigated herein, often lead to a very high number of stirrups; thus, their installation should be checked. As a matter of fact, Fig. 10 shows a possible reinforcement layout within the joint panel for the joints with the highest number of stirrups is required by each code. It can be noted that, assuming the same number of legs and the same diameter of stirrup, EC8 and NZS resulted in a higher spacing respect to those designed according to ACI. The latter resulted in the lowest spacing between joint transverse reinforcement with a minimum clear distance of about 20 mm. This does not comply with ACI requirements suggesting a minimum clear spacing of 1 inch. Also note that in re-designing the joints according to the different codes, the geometry and mechanical properties are not changed to allow a direct comparison with the

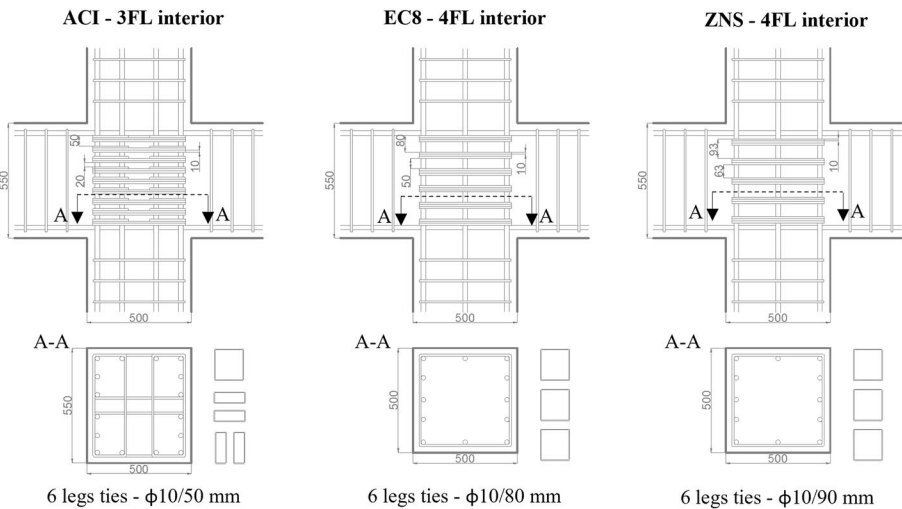


**Fig. 10** Reinforcement layout in joints 3FL-int (designed according to ACI-318) and 4FL-int (designed according to EC8 or NZS) (dimensions in mm)



results of the 2015-test, whereas, in a real application, it would be possible to consider an enlargement of the joint area to allow an easier installation of transverse reinforcements.

## 4 Numerical structural response depending on the design prescriptions for stirrups

The effect of design prescriptions for stirrups in joints on the seismic response of the 10-storey 2015-E-Defense building is numerically investigated in this section. The adopted numerical model will be first described and then applied assuming that the only variable is the joints transverse reinforcement designed according to the different codes (AIJ 2010; EC8, 2005; NZS 2006 or ACI 2019). Joint geometrical properties are kept constant and equal to those of the 2015-E-Defense test.

### 4.1 Adopted modelling approach

A three-dimensional numerical model able to explicitly catch the beam–column joints response is used to simulate the response of the 10-storey 2015-E-Defense building under imposed ground motions. A structural model of the specimen is built starting from the foundation beams (i.e., above the slipping interface in the BS test). Thus, nonlinear dynamic analyses are carried out imposing at the base of the model the displacement time-histories measured at the level of foundation beams. OpenSees platform (McKenna 2010) is used in this work, as described in Di Domenico et al. (2023), where all details about modelling can be found. Herein a brief overview of the nonlinear model is provided to lastly focus the attention on the joint response.

The RC foundation beams are modeled as elastic elements (*ElasticBeamColumn Element* in OpenSees), simply supported at the intersection points between foundation beams and columns/shear walls. Their cross-section and material properties are defined based on available information and technical drawings by Tosauchi et al. (2017) and Kajiwara et al. (2021).

The RC walls are modelled by using a fiber-based approach. A *Force-Based Element* formulation is used with five Gauss–Lobatto integration points. The wall cross-sections are discretized into  $10 \times 30$  fibers for the core, and  $3 \times 9$  fibers for the cover. The confining effect of transverse reinforcement at the wall web is neglected. Longitudinal reinforcements are modelled by means of straight layers of equivalent thickness.

An empirical lumped plasticity approach is used for beams and columns, by implementing a nonlinear spring at both ends of each beam/column, including shear and/or bar slip contribution to the overall members deformability. The elastic part of columns and beams is modelled with an *ElasticBeamColumn Element*. The nonlinear spring is modelled with a *ZeroLength Element*. Beams and columns are assumed as flexural members because the proper design of transverse reinforcement in all members of the specimens prevented shear failures. The empirical moment-chord rotation (envelope and cyclic) response proposed by Haselton et al. (2008) is adopted, slightly modified in the ascending branch to also include the cracking point (assigning a *Parallel Material* in OpenSees to the *ZeroLength Elements* introduced above, as described in Di Domenico et al. 2023 in more detail). Hence, in the adopted modeling approach the axial force-bending moment interaction is explicitly considered only for the RC walls, because their response is expected to be particularly influenced by this phenomenon. The comparison between the observed experimental results and the response predicted through this modeling approach highlighted a quite good predictive

capacity (generally not lower than a modeling approach including fiber-based elements for beam and column elements that consider the axial load-bending moment interaction), thus supporting the modeling assumptions described in Di Domenico et al. (2023).

Second order effects are also considered by means of corotational transformation in OpenSees. Lastly, the behavior of beam–column joints is modeled using the “scissor model” approach proposed by Alath and Kunnath (1995) for both bending direction—see Fig. 11a. Rigid offsets are introduced at the intersections between different structural members (defined as *JointOffset* in *geomTransf* attribute of beams and columns in OpenSees); they cover the joint panel width and height. Rotational springs are implemented between beams and columns rigid offsets at their centerlines intersections (Fig. 11a)—defined by means of a *ZeroLength* element in OpenSees, and characterized by means of the *Pinching4 uniaxial material*. In several studies from the literature (e.g., Celik and Ellingwood 2008; Kim and LaFave 2012; Jeon et al. 2014), such a spring is characterized by a quadri-linear moment ( $M_j$ ) – rotation ( $\Theta_j$ ) relationship, derived from the joint panel shear stress ( $\tau_j$ )—shear strain ( $\gamma_j$ ) response and made up of four characteristic points (Fig. 11b): cracking, pre-peak, peak and residual (or “ultimate”). Note that the chord rotation is assumed equal to the shear strain, and the joint moment  $M_j$  is derived from joint shear stress  $\tau_j$  based on equilibrium equations, as in Celik and Ellingwood (2008).

Different works from the literature studied beam–column joints under seismic action, generally distinguishing between interior and exterior joints, and between reinforced and unreinforced joints. Several works focused on the assessment of joint shear strength only, considering, mechanically or empirically, the contribution of joint stirrups to its strength (e.g. Hwang and Lee 1999; Vollum and Newman 1999; Fardis 2021, among many others). Fewer works focused on the definition of the whole nonlinear response of reinforced joints, namely on the above-mentioned four characteristic points and on the relevant hysteretic response (e.g., Kim and LaFave 2012; Jeon 2013).

Herein, the nonlinear joint shear stress-shear strain relationship is assessed according to Kim and LaFave (2012)’s proposal, which was derived from the analysis of a wide database of experimental tests on beam–column joints reinforced with stirrups. According to this empirical model, the joint shear strength ( $\tau_{j,peak,model}$ ) and corresponding joint shear strain ( $\gamma_{j,peak,model}$ ) are obtained by means of empirical equations (see Eqs. 1 and 2), depending on some key parameters: the joint typology (i.e., interior or exterior, through the parameter JP), the number of beams converging in the joint (through the parameter TB), the amount of transverse reinforcement in the joint (through the joint transverse reinforcement ratio, JI), the longitudinal reinforcement in beams (through the beam longitudinal reinforcement ratio, BI),

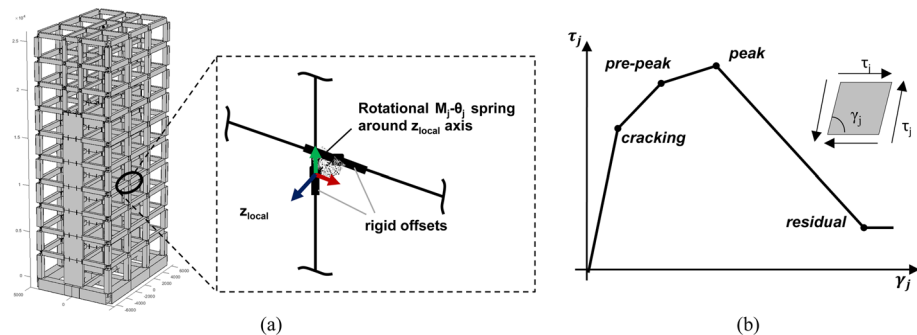


**Fig. 11** Adopted numerical model for beam–column joints (a); nonlinear envelope for joint response (b)

the joint geometrical properties (through the parameter JPRU)/beams eccentricity ( $e$ ), and the concrete compressive strength ( $f_c$ ).

$$\tau_{j,peak,model} = 1.21 \cdot TB^{0.98} \left(1 - \frac{e}{b_c}\right)^{0.68} JI^{0.14} BI^{0.30} JP^{1.33} f_c^{0.76} \text{ (MPa)} \quad (1)$$

$$\gamma_{j,peak,model} = 0.057 \cdot BI \left(1 - \frac{e}{b_c}\right)^{-0.63} JI^{0.098} TB^{1.85} JPRU^{2.11} \left(\frac{\tau_{j,peak}}{f_c}\right)^{-1.75} \text{ (rad)} \quad (2)$$

Key parameters defining the joint response according to the adopted model are summarized in Table 5, considering the different number of stirrups designed according to the selected codes, along with the predicted failure mode (namely joint shear failure expected after beam—BJ—or column—CJ—yielding) for both signs of the acting bending moment on the beam (clockwise,  $M_{CW}$ , or counter-clockwise bending moment,  $M_{CCW}$ ).

**Table 5** Main parameters adopted to define joints' response (frame-direction) and failure mode

Floor	Joint	Type	JP	TB	e	J <sub>I,IIJ</sub>	J <sub>I,EC8</sub>	J <sub>I,ACI</sub>	J <sub>I,NZS</sub>	BI	JPRU	Failure Mode	
												M <sub>CW</sub>	M <sub>CCW</sub>
2FL	A1, A4, D1, D4	Ext	0.75	1	0	0.009	0.013	0.074	0.024	0.125	0.490	BJ	BJ
	A2, A3, D2, D3	Int	1	1	0	0.009	0.013	0.074	0.043	0.102	0.833	BJ	BJ
3FL	A1, A4, D1, D4	Ext	0.75	1	0	0.008	0.012	0.074	0.021	0.110	0.490	BJ	BJ
	A2, A3, D2, D3	Int	1	1	0	0.008	0.013	0.074	0.038	0.090	0.833	BJ	BJ
4FL	A1, A4, D1, D4	Ext	0.75	1	0	0.012	0.024	0.074	0.031	0.136	0.490	BJ	BJ
	A2, A3, D2, D3	Int	1	1	0	0.012	0.057	0.074	0.057	0.122	0.833	BJ	BJ
5FL	A1, A4, D1, D4	Ext	0.75	1	0	0.014	0.040	0.074	0.029	0.144	0.490	BJ	BJ
	A2, A3, D2, D3	Int	1	1	0	0.014	0.045	0.074	0.053	0.128	0.833	BJ	BJ
6FL	A1, A4, D1, D4	Ext	0.75	1	0	0.015	0.051	0.074	0.031	0.153	0.490	BJ	BJ
	A2, A3, D2, D3	Int	1	1	0	0.015	0.081	0.074	0.071	0.136	0.833	BJ	BJ
7FL	A1, A4, D1, D4	Ext	0.75	1	0	0.013	0.009	0.074	0.027	0.117	0.490	BJ	BJ
	A2, A3, D2, D3	Int	1	1	0	0.013	0.037	0.074	0.049	0.102	0.833	BJ	BJ
8FL	A1, A4, D1, D4	Ext	0.75	1	0	0.014	0.009	0.074	0.021	0.103	0.490	BJ	BJ
	A2, A3, D2, D3	Int	1	1	0	0.014	0.008	0.074	0.038	0.080	0.833	BJ	BJ
9FL	A1, A4, D1, D4	Ext	0.75	1	0	0.013	0.009	0.074	0.015	0.079	0.490	BJ	BJ
	A2, A3, D2, D3	Int	1	1	0	0.013	0.018	0.074	0.038	0.079	0.833	BJ	BJ
	B1, B4, C1, C4	Ext	0.75	1.2	0	0.013	0.046	0.103	0.015	0.068	0.490	CJ	BJ
	B2, B3, C2, C3	Int	1	1.2	0	0.013	0.018	0.103	0.028	0.068	0.833	CJ	CJ
10FL	A1, A4, D1, D4	Ext	0.75	1	0	0.017	0.011	0.072	0.020	0.121	0.490	BJ	BJ
	A2, A3, D2, D3	Int	1	1	0	0.017	0.019	0.072	0.037	0.104	0.833	BJ	BJ
	B1, B4, C1, C4	Ext	0.75	1.2	0	0.017	0.011	0.101	0.020	0.104	0.490	CJ	CJ
	B2, B3, C2, C3	Int	1	1.2	0	0.017	0.034	0.101	0.037	0.104	0.833	CJ	CJ
RFL	A1, A4, D1, D4	Ext	0.5	1	0	0.018	0.012	0.072	0.021	0.108	0.269	CJ	BJ
	A2, A3, D2, D3	Int	1	1	0	0.018	0.012	0.072	0.039	0.108	0.269	CJ	CJ
	B1, B4, C1, C4	Ext	0.5	1.2	0	0.018	0.012	0.101	0.021	0.108	0.269	CJ	CJ
	B2, B3, C2, C3	Int	1	1.2	0	0.018	0.012	0.101	0.039	0.108	0.269	CJ	CJ

**Table 6** Parameters used for Pinching4 material in OpenSees for beam–column joints

	rDisp		rForce		uForce		gK1	gD1	gF1
	pos	neg	pos	neg	pos	neg			
Exterior	0.26	0.25	0.20	0.21	− 0.01	− 0.01	1.00	0.24	0.00
Interior	0.25	0.25	0.25	0.26	0.00	0.00	0.93	0.29	0.00

[gK2, gK3, gK4, gK5]=[0.00, 0.10, 0.00, 0.95]; [gD2 gD3 gD4 gD5]=[0.00, 0.15, 0.00, 0.95]; [gF2 gF3 gF4 gF5]=[0.0, 0.0, 0.0, 0.0]

It can be noted that the adopted empirical model neglects the eventual effect of axial load on joint response. Based on the statistical analysis of a wide database of experimental tests on beam–column joints, Kim and LaFave (2012) found that column axial load does not significantly affect joint shear strength or joint shear strain.

A modification of the original Kim and LaFave model is applied herein, particularly concerning joint strength. It is worth noting that shear strength models in the literature are calibrated or validated by means of experimental tests mostly performed under mono-directional loadings. Very recent studies from literature showed that joint shear strength under bi-directional loading, like that suffered by joints in 2015 E-Defense tests, can be significantly lower than the relevant strength of the same joint under mono-directional loading. Han and Lee (2020) quantified this effect for corner joints experimentally, finding that such a strength reduction can reach − 30%. Based on this outcome, a common reduction factor equal to 0.7 (to be multiplied by the Kim and LaFave’s strength) is used for all joints in the adopted model.

Finally, it should be noted that the peak load moment determined from the predicted (empirical) joint shear strength ( $M_{j,max,model}$ ) should be furtherly limited to the flexural strength ( $M_{j,flex}$ ) of adjacent beams/columns (which cannot be even overcome), according to Celik and Ellingwood (2008), namely the peak load moment to be used in the numerical model for each joint ( $M_{j,max}$ ) can be computed as follows (Eq. 3):

$$M_{j,max} = \min(M_{j,max,model}; M_{j,flex}) = \min\left(M_{j,max,model}; \min\left(\sum_i M_{beam,flex,i}; \sum_j M_{col,flex,j}\right)\right) \tag{3}$$

where  $M_{beam,flex,i}$  and  $M_{col,flex,j}$  represent the flexural strength of the *i*th converging beam and the *j*th converging column, respectively.

Joint shear stress and shear strain at cracking, pre-peak and “ultimate” points are then derived by multiplying joint shear stress and strain at peak point by empirically calibrated factors (Kim and LaFave 2012).

Hysteretic degradation in the cyclic response is also considered as suggested by Jeon (2013), thus using sets of the parameters for *Pinching4 uniaxial material* describing hysteretic response that are different for exterior and interior joints. They describe the position of pinching breakpoints (rDisp, rForce and uForce), the unloading stiffness degradation (gK<sub>i</sub>), and the reloading stiffness degradation (gD<sub>i</sub>), as shown in Table 6. No strength degradation is implemented (i.e., parameters gF<sub>i</sub> are imposed herein equal to zero), since the  $M_j-\theta_j$  response coming from Kim and LaFave’s model already represent the envelope of cyclically degraded nonlinear response.

Figure 12 shows the resulting moment-rotation envelopes for joints from 1st to the 6th floor, in the frame direction, depending on the code adopted for joints stirrups

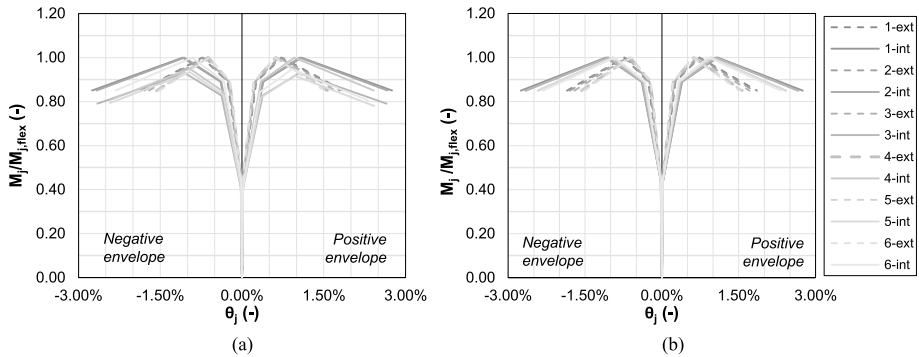


**Fig. 12** Joint moment-rotation envelopes obtained for stirrups designed according to AIJ (2010) (a) and for stirrups designed according to EC8/ACI/NZS (b)—1st to 6th floor, frame direction

design. In this figure, the joint moment is divided by the flexural strength of the adjacent beams/columns to emphasize what follows. If stirrups designed according to AIJ (2010) prescriptions are used, in most cases, joint maximum moment ( $M_{j,max}$ ) is determined by the converging beams/columns flexural strength ( $M_j/M_{j,flex}$  in Fig. 12 equal to 1), except than for some joints in low-intermediate floors. On the contrary, when  $\rho_{jh}$  is defined according to all the other codes considered herein (EC8, NZS and ACI),  $M_{j,max,model}$  generally results higher than the relevant joint strength obtained with AIJ-compliant stirrups, and  $M_{j,max}$  is always provided by the converging beams/columns flexural strength ( $M_j/M_{j,flex}$  in Fig. 10 is always equal to 1). As a result,  $M_{j,max}$  is slightly higher (from +5 to +9%) for EC8/ACI/NZS-compliant stirrups with respect to joints with AIJ-compliant stirrups, for some joints from the 3rd to the 6th floor (the mostly damaged in 2015-E-Defense tests). Additionally, it can be noted that joints generally reach their peak load for shear strain in the range 0.5–1.0% (with lower values for exterior joints with respect to the interior ones), with not significant difference between AIJ-compliant and EC8/ACI/NZS-compliant stirrups in joints. A wider range of shear strain (1.5–2.8%) characterizes the achievement of the “residual” point.

It is worth mentioning here that a slight simplification is introduced in modeling the joint with stirrups designed according to EC8/ACI/NZS. As a matter of fact, such codes always lead to a higher number of stirrups in joints with respect to AIJ for the prototype building, but each code provides a different transverse reinforcement percentage. EC8, ACI, and NZS produce the same increase in joint strength, as commented above, but they would also lead to a bit different joint deformability. According to Kim and LaFave’s model, joint shear strain at peak load (and, in tune, joint shear strain at all the other characteristic points of the joint response) changes as a function of  $\rho_{jh}$  (see Eq. 2). As a result, a slight reduction in  $\gamma_{j,peak,model}$  would be obtained with respect to the case AIJ-compliant stirrups, for EC8, ACI, and NZS-compliant stirrups. Nevertheless, in the following models, the same joint shear strain values are used in defining the joint response for all codes, for sake of simplification. It is worth noting that, as shown in what follows, joint deformability demand is always very small (never beyond the pre-peak point of the joint response) for EC8/ACI/NZS-model, thus proving that the adopted simplification does not affect significantly the final numerical results.

In summary, two 3D nonlinear models are implemented in OpenSees: the first one with AIJ (2010)-compliant joints stirrups, and the another one with EC8/ACI/NZS-conforming stirrups in joints. Each model is tested by applying at its base the three displacement components (two horizontal components plus the vertical one) of the Kobe earthquake recorded during the tests, as explained in Di Domenico et al. (2023). The main results of such numerical analyses are shown in the following sub-section. On the prediction capability of the adopted model, for what concern the AIJ-compliant stirrups (that is the 2015-E-Defense test), refer to Di Domenico et al. (2023).

### 4.2 Numerical results: AIJ- vs- EC8/NZS/ACI design for joint stirrups

The numerical results obtained for the two models mentioned above are reported in this section, first in terms of maximum achieved IDR ( $IDR_{max}$ ) at each story (see Fig. 13). An additional term of comparison is also analyzed, namely the relevant 3D-model characterized by a linear elastic behavior of beam–column joints, where joint elastic stiffness simply reflects the shear stiffness of the joint panel. Again, the frame direction only is investigated, where joints resulted more damaged in 2015-E-Defense tests and where monitored joints were available (see Sect. 2.1).

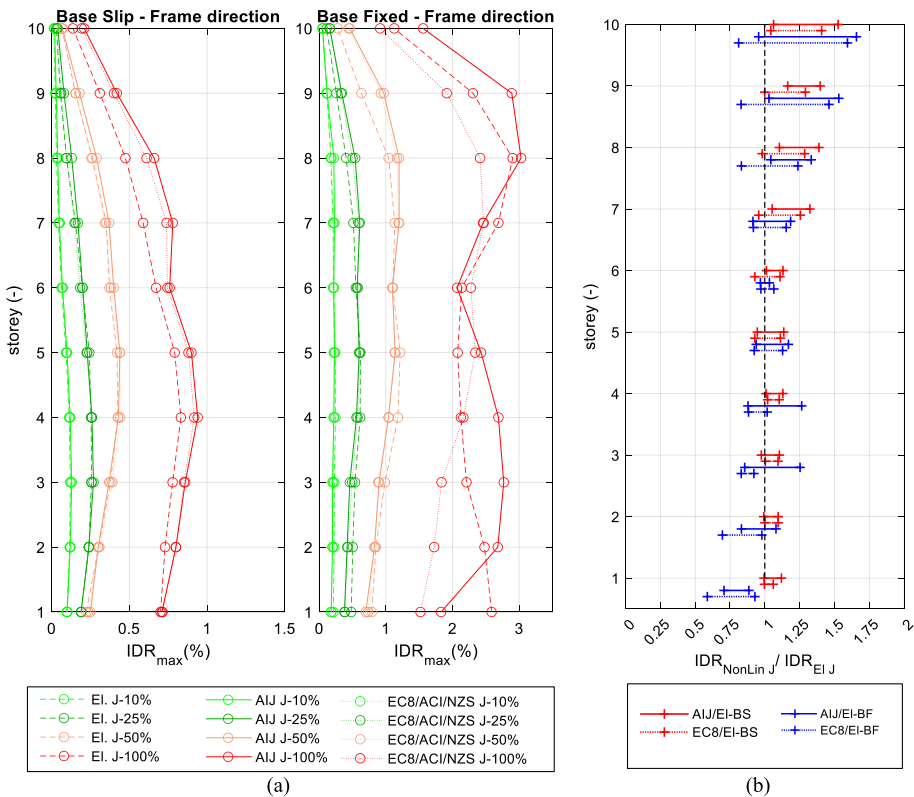


**Fig. 13** Influence of the stirrups design in joints on the maximum IDR demand (a) and comparison between nonlinear joint with AIJ- or EC8/ACI/NZS-compliant stirrups in joints and elastic (EI) joints—min–max ranges (b). (EC8/ACI/NZS- is shortened in this figure as “EC8”)

Figure 13 shows that, for BS-tests, when joints are modelled as linear elastic members (“El J”), the maximum IDR demand is generally lower with respect to the nonlinear modelling of joints, for both models (AIJ- or EC8/ACI/NZS- compliant stirrups). This is also true, in most cases for BF tests, especially at the higher stories at the lower shaking intensities. At the highest intensities such an outcome becomes more difficult to explain looking at joints’ response only, since a significant nonlinear demand affects also beams and columns ends. In summary, the ratio between IDR demand related to nonlinear joints modelling and IDR demand related to linear elastic joints modelling ranges between 0.59 and 1.66 (see Fig. 13b), thus proving that considering the “real” behavior of beam–column joints in modelling is certainly paramount for an accurate numerical prediction. Additionally, when AIJ-compliant stirrups in joints are considered the maximum IDR demand is generally higher than that obtained for EC8/ACI/NZS-compliant stirrups in joints. Numerical results obtained for the above-mentioned 3D models are also expressed in Fig. 14 in terms of maximum joint shear strain ( $\gamma_{j,max}$ ) for those (interior) joints in the frame direction that were monitored during the experimental phases (see Sect. 2.1). In case of elastic joints,  $\gamma_{j,max}$  values are always very small, and, thus, joints contribution to the overall IDR demand is negligible. On the contrary, AIJ-J and EC8/ACI/NZS-J models provide quite similar  $\gamma_{j,max}$  values for BS-tests; only at the 3rd and the 2<sup>nd</sup> stories AIJ-J model leads to slightly higher  $\gamma_{j,max}$  values at 100% Kobe (namely SF = 1). On the contrary, in the BF-tests,  $\gamma_{j,max}$  values related to AIJ-J model become significantly higher with respect to EC8/ACI/NZS-J model, especially at the highest intensities (100% Kobe). Particularly for BF-test at 100% Kobe, in case of AIJ-J model, most of the monitored joints reach or overcome their peak point according to the adopted model (see Fig. 14b, where the range related to interior joints only is reported in grey), starting to degrade and, thus, affecting the resulting expected damage in joints (as shown in the next section). On the other hand, the EC8/ACI/NZS-J model provides maximum joint shear strain values that are always lower than those corresponding to the peak point according to Kim and LaFave’s model, leading to a lower expected damage level in joints with respect to the AIJ-J model.

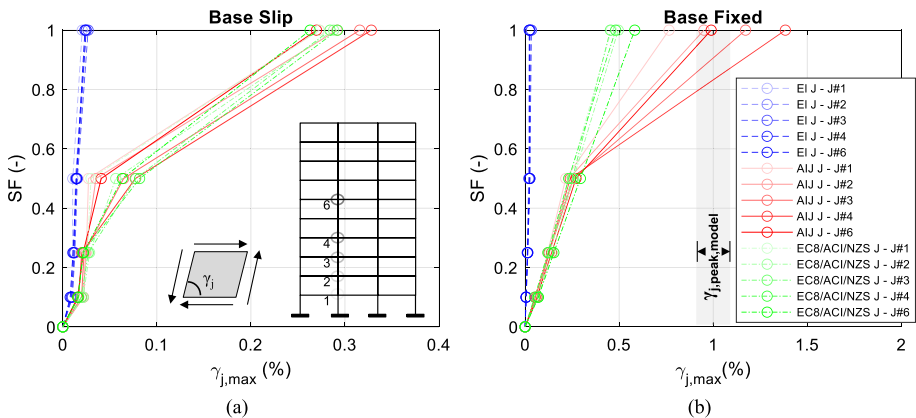


**Fig. 14** Comparison comparison between nonlinear joint (with AIJ- or EC8/ACI/NZS-compliant stirrups in joints) and elastic (EI) joint in terms of maximum joint distortion on the monitored joints (see Sect. 2.1): base slip test (a); base fixed test (b)

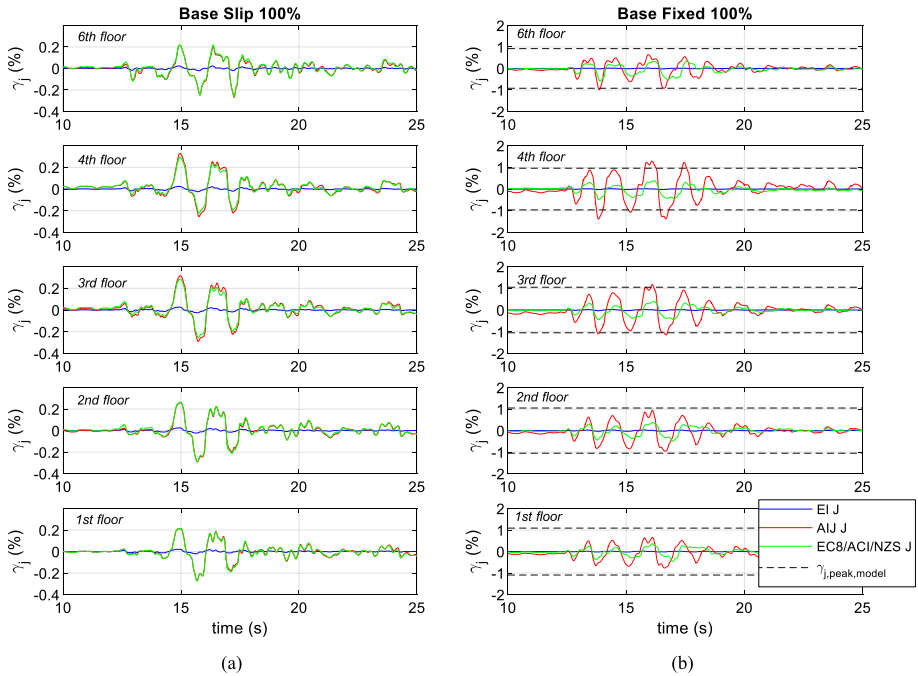


**Fig. 15** Comparison comparison between nonlinear joint (with AIJ- or EC8/ACI/NZS-compliant stirrups in joints) and elastic (EI) joint in terms of joint distortion time history on the monitored joints (see Sect. 2.1), 100% Kobe: base slip test (a); base fixed test (b)

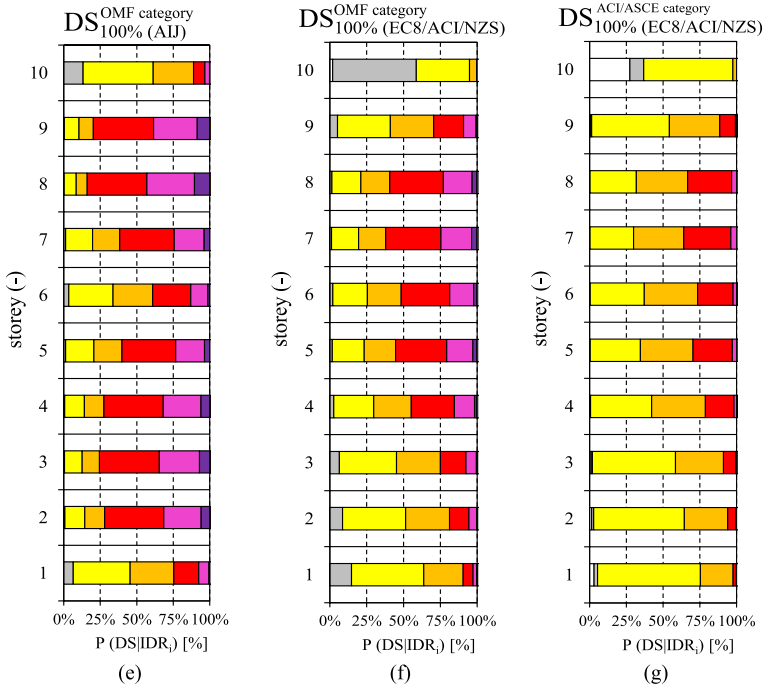
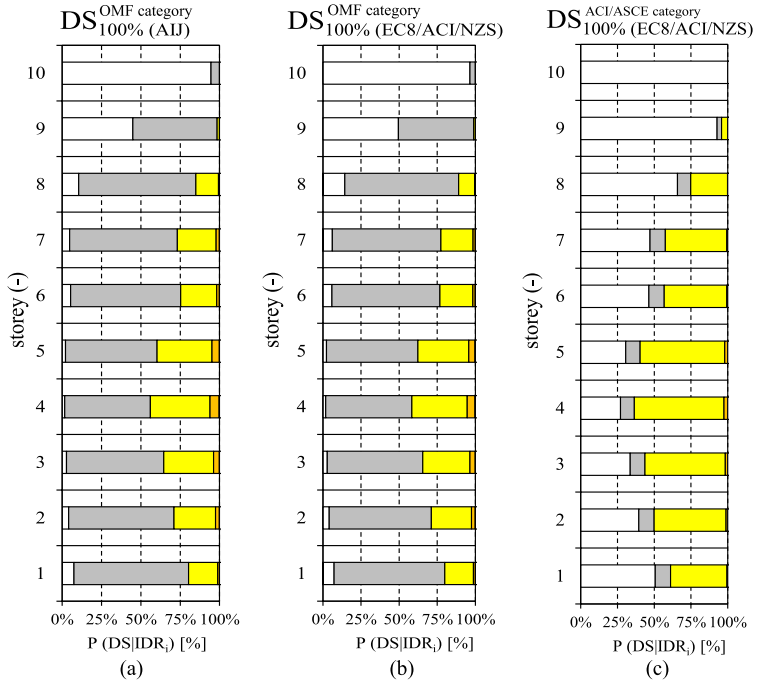
Lastly, Fig. 15 shows the joint shear strain ( $\gamma_j$ ) time history at 100% Kobe for BS- and BF- tests, for the same joints investigated above in the time interval [10; 25] s. It can be noted that trends already commented above for  $\gamma_{j,max}$  still applies for  $\gamma_j$ . Additionally,  $\gamma_j$  peaks during the time history are almost contemporary if AIJ-J and EC8/ACI/NZS-J models are compared, for BS-test. This latter remark generally is less clear for BF-test, especially after the peak joint strain (predicted by the adopted model) is achieved for the AIJ-J model (dotted lines in Fig. 15b), as occurs in joints at the 3rd, 4th and 6th floor.

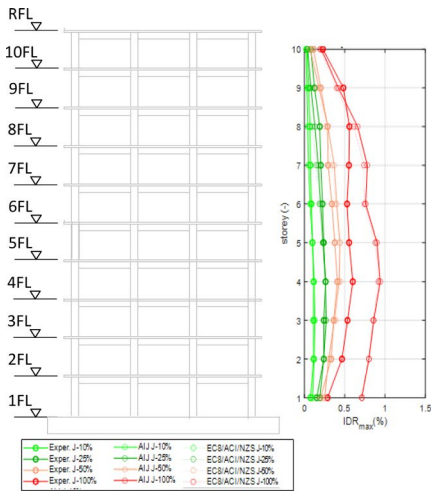
## 5 Damage analysis depending on the design prescriptions for joint stirrups

In this section the results in terms of  $IDR_{max}$  of the numerical analyses conducted by using the different numerical models (with stirrups designed according to ACI or EC8/ACI/NZS standards) are used to assess the attained damage in terms of  $DS_{P_{max}}$ , as performed in Sect. 2.2 based on experimental data. Thus, Fig. 16 shows the probability of occurrence

**Fig. 16** Comparison of predicted DSs by using: BS model with joints designed according to AIJ (a); BS model with joints designed according to EC8/ACI/NZS (b); BS model with joints designed according to EC8/ACI/NZS and DS for ACI/ASCE compliant BCJs (c); BF model with joints designed according to AIJ (e); BF model with joints designed according to EC8/ACI/NZS (f); BF model with joints designed according to EC8/ACI/NZS and DSs for ACI/ASCE compliant BCJs (g)

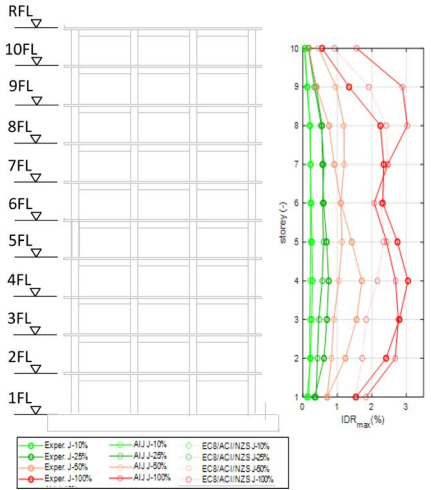






DS <sub>Pmax</sub> OMF category (Exper.)	DS <sub>Pmax</sub> OMF category (AIJ)	DS <sub>Pmax</sub> OMF category (EC8/ACI/NZS)	DS <sub>Pmax</sub> ACI/ASCE cat. (EC8/ACI/NZS)
Null	Null	Null	Null
DSC	DSC	Null	Null
DSC	DSC	DSC	Null
DSC	DSC	DSC	Null
DSC	DSC	DSC	Null
DSC	DSC	DSC	DS0
DSC	DSC	DSC	DS0
DSC	DSC	DSC	DS0
DSC	DSC	DSC	DS0
Null	DSC	DSC	Null
0.60%      0.94%      0.92%      0.92%			
IDR <sub>max</sub>			

(a)



DS <sub>Pmax</sub> OMF category (Exper.)	DS <sub>Pmax</sub> OMF category (AIJ)	DS <sub>Pmax</sub> OMF category (EC8/ACI/NZS)	DS <sub>Pmax</sub> ACI/ASCE cat. (EC8/ACI/NZS)
DSC	DS0	DSC	DS0
DS0	DS2	DS0	DS0
DS2	DS2	DS2	DS1
DS2	DS2	DS2	DS1
DS2	DS2	DS2	DS1
DS2	DS0	DS2	DS1
DS2	DS2	DS2	DS1
DS2	DS2	DS2	DS0
DS2	DS2	DS2	DS0
DS2	DS2	DS0	DS0
DS2	DS2	DS0	DS0
3.05%      3.03%      2.47%      2.47%			
IDR <sub>max</sub>			

(b)

**Fig. 17** Comparison between nonlinear models (with AIJ- or EC8/ACI/NZS-compliant stirrups in joints) and experimental results in terms of attained DS: base slip test (a); base fixed test (b)

of each DS at each floor for 100%-BS and 100%-BF tests when joints stirrups are designed according to AIJ or EC8/ACI/NZS. It is worth noting that two different damage classifications belonging to OMF and ACI/ASCE category of BCJs are considered at this stage. This is to account for the different- and lower- sensitivity to damage of BCJs designed according to EC8/ACI/NZS standards. The resulting DS<sub>Pmax</sub> is reported in Fig. 17. The same results are analysed also for lower intensity as commented below.

The damage analysis of the prototype building in the Base Slip configuration shows very minor differences varying the numerical model of the joint. No significant differences are visible until 100% intensity in term of DS<sub>Pmax</sub>. Additionally, the predicted damage for

the building numerical model where joint stirrups are designed according to AIJ is very close to the actual damage shown in Sect. 2 (Fig. 17a).

With reference to the building in the Base Fixed configuration (Fig. 17b), the DSs assessed considering the results of the numerical model with joints stirrups designed according to AIJ well match those assigned according to experimental results (Fig. 17b). A predominance of DS2 is assessed at 100% Kobe. This matching is confirmed by the good agreement between the predicted  $IDR_{max}$  and the experimental one. Nevertheless, a difference between the experimental observations and numerical model can be observed in terms of the DS distribution along the height. Indeed, the numerical predictions overestimate damage at the highest floors. This is related to the accuracy of the adopted numerical model that provides reliable estimations of the peak IDR while it is less accurate in the prediction of the IDR distribution along the height (see Di Domenico et al. 2023, for more details).

Additionally, assuming that the joint stirrups were designed according to different standards (i.e. ACI, EC8 or NZS), the reduction of the joint shear distortion leads to a decrease of the  $IDR_{max}$  demand at most floors (see Fig. 17b). Assuming the OMF damage classification, this resulted in a reduction of the number of floors where  $DS_{Pmax} = DS2$  and a significant number of floors that experienced a DS0.

It is worth mentioning that comparisons discussed until now are made considering the same damage classification (joint belonging to the OMF-BYJF category, according to Lowes and Li 2009) both for the building with joint designed according to AIJ and other codes (ACI, EC8, NZS). However, as already mentioned above, it should be noted that increasing the ratio of joint transverse reinforcement a change of the damage classification may be needed, especially when joint reinforcement complies with current ACI/ASCE standards. This may have a significant influence on the expected damage since that a ductile failure of the joint subassembly is expected and the onset of a high damage state could be achieved at a median drift higher than non-conforming BCJs. Thus, a further reduction of expected damage (with respect to that estimated herein) could be attained for joints designed with stirrups compliant with EC8/ACI/NZS standards, due not only to a lower drift demand, but also to higher IDR thresholds (lower sensitivity of the joint subassembly to damage). In particular, when IDR thresholds by Lowes and Li (2009) related to ACI Special Moment Frames (SMF) category are used, at 100% Kobe-Base fixed, a predominance of DS0 at the lowest levels (1st to 4th floor) is found. Intermediate floors (5th to 8th) experienced a DS1, while the 9th and 10th floor experienced a DS0. Thus, the use of a more appropriate damage classification outlined a significant reduction of the observed DS with a predominance of DS0 and a maximum of DS1 (see Fig. 17b). This remarks the importance of transverse reinforcement in the seismic response of the joint panel that may significantly contain the joint shear deformation resulting in a reduction of the global drift demand, and, in turn, of the expected maximum DS and its extension. This will have a significant influence on expected losses under earthquake loads (De Martino et al. 2017; De Risi et al. 2020; Del Gaudio et al. 2022).

A summary of the damage analysis commented in this section and in Sect. 2 is presented in Fig. 18, by means of the parameter  $DS^*$ , defined as in Eq. (4), obtained for all models/ experimental data and plotted depending on the input PGA.

$$DS^* = \frac{\sum_{j=1}^{N_s} DS_{Pmax,j}}{N_s} \tag{4}$$

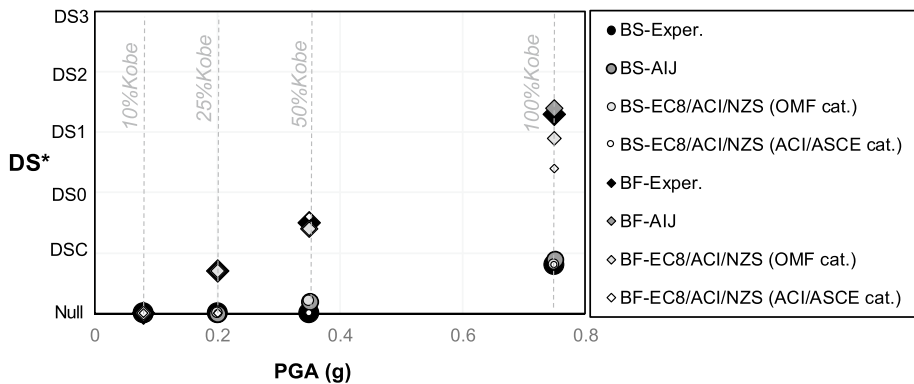


**Fig. 18** Summary of  $DS^*$  obtained for all intensities as a function of the corresponding PGA

The parameter  $DS^*$  represents the average along the building height of the most likely damage at each floor, and thus it considers, in a simplified manner, both maximum damage and damage extension.

For the BS-tests, predicted  $DS^*$  is technically the same for both the numerical models and for damage analysis coming from experimental outcomes, at each intensity; the maximum  $DS^*$  results a cosmetic damage, and it is achieved at 100% Kobe (PGA = 0.75 g). A similar outcome can be observed for BF-tests, except than at 100% Kobe, where a reduction in predicted  $DS^*$  is detected when EC8/ACI/NZS-model results are used, or ACI/ACE damage classification is adopted.

## 6 Conclusions

Beam–column joints (BCJs) in RC buildings are often significantly damaged during seismic shakings, especially in absence of a proper design of joints dimensions and stirrups. The 10-storey building tested at E-Defense in 2015—tested in a base-slip, BS, and a base-fixed, BF, condition—was an evident proof of the role of joints response and damage to the global behavior of the building. Indeed, when cast-iron plates were activated at the base of the building, the observed damage was always very low, from 10 to 100% Kobe earthquake, thus proving the efficiency of the adopted base isolation system. On the contrary, when 50–100% Kobe earthquake was applied to that building in a fixed-base condition, the main damage was observed in BCJs, which showed wide diagonal cracks and concrete cover spalling. Assessing the damage in joint sub-assemblages according to Lowes and Li (2009) damage metric, expressed in terms of IDR thresholds, only cosmetic repair (DSC) or repair of plaster and finishes (DS0) could be needed after BS-tests, whereas, during the BF-test at 100% Kobe, the intermediate floors (3rd to 5th) experienced a moderate to heavy damage (DS2/DS3) in tune with the AIJ damage classification.

Joint stirrups of the 2015-E-Defense building prototype were designed according to the Japanese standard (AIJ 2010), which suggested to reinforce joint panels with the 0.2% of geometric transverse reinforcement ratio. In this paper, the European (EC8, 2004), American (ACI 2019) and New Zealand (NZS 2006) standards are used to re-design the joint stirrups of the prototype building (keeping constant the mechanical and geometric properties). Because these code prescriptions rely on different theoretical approaches,

a different geometric transverse reinforcement ratio is found. However, it is always significantly higher than 0.2% used in the prototype building.

Thus, a 3D numerical model was implemented in OpenSees platform to reproduce the 10-storey building response and to simulate its behavior depending on the stirrups amount located in BCJs. A lumped-plasticity approach was used for beams and columns, a fiber sections with an associated plastic hinge length was implemented for RC walls, and a scissors-model was used for BCJs. Kim and LaFave (2012)'s model was implemented to reproduce the BCJs monotonic response, reducing the empirical predicted strength to consider the contemporary biaxial loading, and limiting it to the flexural strength of the adjacent beams/columns. As a result of these assumptions, when AIJ-based design is adopted for stirrups in BCJs, Null damage or DSC are predicted for the BS tests, and a maximum damage DS3 for BF-100% Kobe is obtained, as actually observed during the experimental tests (even if with some difference in the floor at which the maximum damage is achieved).

The use of larger number of joint stirrups designed according to other international standards (i.e. ACI, EC8 or NZS) results in a reduction in the joint shear distortion leading to a decrease of the maximum IDR demand at all the floors. In tune, the expected damage can be classified as DS0 with peak of DS2 at most of the floors by using the same damage classification (OMF-BYJF) used for the reference building. Thus, a reduction of the number of floors where the maximum damage level is attained (namely a reduction of the damage extension along the building height) has a direct effect in terms of reduction of the expected seismic losses for the prototype building. This result is even more clear when a different and more appropriate damage classification (ACI/ASCE) is used for the building with BCJs designed according to the EC8/ACI/NZS codes. In this case a predominance of DS0, with some floors at DS1, is found.

The above discussed outcomes clearly highlight that a proper amount of transverse reinforcement in BCJs may significantly reduce the joint shear strain demand and, in tune, the overall drift demand, leading to a reduction of the expected damage. This outcome should be carefully considered following a design oriented to the damage containment in modern RC buildings that can be easily repaired even after severe ground shakings without the need of expensive refurbishment or demolition. It is worth mentioning that use a large amount of joint transverse reinforcement should be balanced by the need of an easy installation of these reinforcement in practical applications.

**Authors contributions** All authors contributed to the study conception and design. All authors read and approved the final manuscript.

**Funding** Open access funding provided by Università degli Studi di Napoli Federico II within the CRUI-CARE Agreement. The support of ReLUIIS-DPC 2019–2021 and 2022–2023 research programs, funded by the Presidenza del Consiglio dei Ministri—Dipartimento della Protezione Civile (DPC), is gratefully acknowledged.

**Data availability** The data generated during the current study are available from the corresponding author on reasonable request.

## Declarations

**Conflict of interest** The authors have no relevant financial or non-financial interests to disclose.

**Open Access** This article is licensed under a Creative Commons Attribution 4.0 International License, which permits use, sharing, adaptation, distribution and reproduction in any medium or format, as long as you give appropriate credit to the original author(s) and the source, provide a link to the Creative Commons licence,

and indicate if changes were made. The images or other third party material in this article are included in the article's Creative Commons licence, unless indicated otherwise in a credit line to the material. If material is not included in the article's Creative Commons licence and your intended use is not permitted by statutory regulation or exceeds the permitted use, you will need to obtain permission directly from the copyright holder. To view a copy of this licence, visit <http://creativecommons.org/licenses/by/4.0/>.

## References

- ACI-ASCE 352 (1976) Recommendations for Design of Beam–Column Joints for Monolithic Concrete Structures. Detroit, MI, USA
- ACI 318-11 (2011) Building code requirements for structural concrete and commentar. Farmington Hills, MI, USA
- ACI 318 (1995) Building code requirements for structural concrete. Farmington Hills, MI, USA
- ACI 318 (2019) Building code requirements for structural concrete and commentary
- AIJ (1989) Design guidelines for earthquake resistant RC buildings based on the ultimate strength concept. Architectural Institute of Japan, Tokyo, Japan
- AIJ (2010) AIJ standard for structural calculation of reinforced concrete structures revised 2010. Architectural Institute of Japan
- Alath S, Kunnath SK (1995) Modelling inelastic shear deformation in RC beam–column joints. In: Engineering mechanics proceedings of 10th conference, May 21–24, University of Colorado at Boulder, Boulder, Colorado, ASCE, New York
- Applied Technology Council (2012) FEMA P-58–4: seismic performance assessment of buildings. Fema P-58-4 1
- Brown PC, Lowes LN (2007) Fragility functions for modern reinforced-concrete beam–column joints. *Earthq Spectra* 23:263–289. <https://doi.org/10.1193/1.2723150>
- Bruneau M, MacRae G (2019) Building structural systems in Christchurch's post-earthquake reconstruction. *Earthq Spectra* 35:1953–1978. <https://doi.org/10.1193/052818EQS1260>
- Cardone D (2016) Fragility curves and loss functions for RC structural components with smooth rebars. *Earthq Struct* 10:1181–1212. <https://doi.org/10.12989/eas.2016.10.5.1181>
- Celik OC, Ellingwood B (2008) Modeling beam–column joints in fragility assessment of gravity load designed reinforced concrete frames. *J Earthq Eng* 35:357–381
- CEN (2004) EN1998 Eurocode 8: Design of structures for earthquake resistance—part 1: general rules, seismic actions and rules for buildings
- Cuevas A, Pampanin S (2017) Post-seismic capacity of damaged and repaired reinforced concrete plastic hinges extracted from a real building. *World Conf Earthq Eng* 3142:1–13
- Del Gaudio C, De Risi MT, Verderame GM (2022) Seismic loss prediction for infilled RC buildings via simplified analytical method. *J Earthq Eng* 26(11):5477–5510
- De Martino G, Di Ludovico M, Protà A, Moroni C, Manfredi G, Dolce M (2017) Estimation of repair costs for RC and masonry residential buildings based on damage data collected by post-earthquake visual inspection. *Bullet Earthq Eng* 15:1681–1706
- De Risi MT, Del Gaudio C, Verderame GM (2020) A component-level methodology to evaluate the seismic repair costs of infills and services for Italian RC buildings. *Bullet Earthq Eng* 18:6533–6570
- Del Vecchio C, Di Ludovico M, Protà A (2020) Repair costs of reinforced concrete building components: from actual data analysis to calibrated consequence functions. *Earthq Spectra* 36:1–25. <https://doi.org/10.1177/8755293019878194>
- Di Domenico M, Gaetani d'Aragona M, Polese M, Magliulo G, Protà A, Verderame GM, Kajiwara K (2023) Nonlinear modeling of the ten-story RC building at E-Defense (2015): assessment with different modeling assumptions. *Bull Earthq Eng*. <https://doi.org/10.1007/s10518-023-01627-9>
- Di Ludovico M, Protà A, Moroni C et al (2017) Reconstruction process of damaged residential buildings outside the historical centres after L'Aquila earthquake—part II: “heavy damage” reconstruction. *Bull Earthq Eng* 15:693–729. <https://doi.org/10.1007/s10518-016-9979-3>
- Fardis MN (2021) Shear strength model for RC joints, consistent with the shear design rules for prismatic members in the second-generation Eurocodes. *Bull Earthq Eng* 19:889–917
- Fardis MN (2009) Seismic design, assessment and retrofitting of concrete buildings (based on EN-Eurocode 8), geotechnic. Springer, Berlin
- Favvata MJ, Karayannis CG (2014) Influence of pinching effect of exterior joints on the seismic behavior of RC frames. *Earthq Struct* 6(1):089–110. <https://doi.org/10.12989/eas.2014.6.1.089>

- Favvata MJ, Izzuddin BA, Karayannis CG (2008) Modelling exterior beam–column joints for seismic analysis of RC frame structures. *Earthq Eng Struct Dyn* 37:1527–1548. <https://doi.org/10.1002/eqe.826>
- Galvis FA, Miranda E, Heresi P et al (2020) Overview of collapsed buildings in Mexico City after the 19 September 2017 (Mw7.1) earthquake. *Earthq Spectra* 36:83–109. <https://doi.org/10.1177/8755293020936694>
- Guimaraes GN, Kreger ME, Jirsa JO (1989) PMFSEL report: reinforced concrete frame connections constructed using high-strength materials
- Hakuto S, Park R, Tanaka H (2000) Seismic load tests on interior and exterior beam–column joints with substandard reinforcing details. *ACI J* 1
- Han SW, Lee CS (2020) Cyclic behavior of RC OMF beam–corner column joints under unidirectional and bidirectional loadings. *Eng Struct* 224:111304
- Haselton CB, Leil AB, Lange ST, Deierlein GD (2008) PEER report 2007/03: beam–column element model calibrated for predicting flexural response leading to global collapse of RC frame buildings. Berkeley, California
- Hwang SJ, Lee HJ (1999) Analytical model for predicting shear strengths of exterior reinforced concrete beam–column joints for seismic resistance. *ACI Struct J* 96:846–857
- Izzuddin BA (2009) ADAPTIC: a program for the adaptive analysis of space frames. ESEE-89/7 Imperial College, London, UK. <https://doi.org/10.25561/4228>
- JBDPA (2015) Japan Building Disaster Prevention Association—Guideline for Post-earthquake Damage Evaluation and Rehabilitation (in Japanese). Japan
- Jeon JS (2013) Aftershock vulnerability assessment of damaged reinforced concrete buildings in California (Doctoral dissertation, Georgia Institute of Technology)
- Jeon JS, Shafieezadeh A, DesRoches R (2014) Statistical models for shear strength of RC beam–column joints using machine-learning techniques. *Earthq Eng Struct Dyn* 43:2075–2096. <https://doi.org/10.1002/eqe>
- Kajiwara K, Tosachi Y, Do Kang J et al (2021) Shaking-table tests of a full-scale ten-story reinforced-concrete building (FY2015) Phase I: free-standing system with base sliding and uplifting. *Eng Struct* 233:111848. <https://doi.org/10.1016/j.engstruct.2020.111848>
- Kajiwara K, Tosachi Y, Sato E et al (2017) 2015 Three-dimensional shaking table test of a 10-story reinforced concrete building on the E-Defense part 1: overview and specimen design of the base slip and base fixed tests. In: 16th world conference on earthquake engineering Santiago, Chile, 9–13 January Paper No 4:1–9
- Kam WY, Pampanin S, Elwood K (2011) Seismic performance of reinforced concrete buildings in the 22 February Christchurch (Lyttelton) earthquake. *Bull N Zeal Soc Earthq Eng* 44:239–278. <https://doi.org/10.5459/bnzsee.44.4.239-278>
- Kim J, LaFave JM (2012) A simplified approach to joint shear behavior prediction of RC beam–column connections. *Earthq Spectra* 28:1071–1096. <https://doi.org/10.1193/1.4000064>
- Lan YJ, Stavridis A, Kim I et al (2020) ATC Mw7.1 Puebla-Morelos earthquake reconnaissance observations: structural observations and instrumentation. *Earthq Spectra* 36:31–48. <https://doi.org/10.1177/8755293020977520>
- Lehman DE, Stanton J, Anderson M et al (2004) Seismic performance of older beam–column joints. In: Proceedings of 13th World Conference on Earthquake Engineering 1464
- Leon RT, Kam WY, Pampanin S (2012) Performance of beam–column joints in the 2010–2012 Christchurch earthquakes. *Am Concr Inst ACI Spec Publ* 47–66
- Lowes LN, Li J (2009) Fragility functions for concrete moment frames. Redwood City, California 94065
- Maeda M, Kang DE (2009) Post-earthquake damage evaluation of reinforced concrete buildings. *J Adv Concr Technol* 7:327–335. <https://doi.org/10.3151/jact.7.327>
- McKenna F (2010) OpenSees: a framework for earthquake engineering simulation. *Comput Sci Eng* 13:58–66
- Meinheit DF, Jirsa JO (1977) The shear strength of reinforced concrete beam–column joints
- MOW (1976) Ministry of works and development New Zealand: “Code of Practice for Seismic Design Public Buildings”
- Nagae T, Ghannoum WM, Kwon J et al (2015) Design implications of large-scale shake-table test on four-story reinforced concrete building. *ACI Struct J* 112:135–146. <https://doi.org/10.14359/51687421>
- NZS 3101 (1982) Concrete structures standard. New Zealand
- NZS 3101 (1995) Concrete structures standard. New Zealand
- NZS 3101 (2006) Concrete structures standard. New Zealand
- Pagni CA, Lowes LN (2006) Fragility functions for older reinforced concrete beam–column joints. *Earthq Spectra* 22:215–238. <https://doi.org/10.1193/1.2163365>
- Park R (1996) The revised New Zealand concrete design standard. In: Eleventh world conference on Earthquake Engineering, paper No. 622
- Paulay T, Priestley MJN (1992) Seismic design of reinforced concrete and masonry buildings. Wiley, New York

- Ricci P, de Luca F, Verderame GM (2011) 6th April 2009 L'Aquila earthquake, Italy: reinforced concrete building performance. *Bull Earthq Eng* 9:285–305. <https://doi.org/10.1007/s10518-010-9204-8>
- Sato E, Tosauchi Y, Fukuyama K et al (2017) 2015 Three-dimensional shaking table test of a 10-story reinforced concrete building on the E-Defense; Part 2: Specimen Fabrication and Construction, Test Procedure, and Instrumentation Program. In: 16th world conference on earthquake engineering Santiago, Chile, 9–13 January
- Shiohara H (2017) A new AIJ standard for Seismic Capacity Calculation: Recent advances in beam–column joint design and seismic collapse simulation on reinforced concrete frame buildings. *Am Concr Inst ACI Spec Publ*. <https://doi.org/10.14359/51689689>
- Shiohara H, June R (1998) A new model for joint shear failure of reinforced concrete interior beam-to-column joint. *J Sch Eng Univ Tokyo* 45:1–30
- Shiohara H, Kusuhara F (2014) The next generation seismic design for reinforced concrete beam–column joints. In: Tenth US national conference on earthquake engineering. Anchorage, Alaska
- Tosauchi Y, Sato E, Fukuyama K et al (2017) 2015 Three-dimensional shaking table test of a 10-story reinforced concrete building on the E-Defense; Part 3: base slip and base fixed test results. In: 16th world conference on earthquake engineering Santiago, Chile, 9–13 January
- Villalobos E, Sim C, Smith-Pardo JP et al (2018) The 16 April 2016 Ecuador earthquake damage assessment survey. *Earthq Spectra* 34:1201–1217. <https://doi.org/10.1193/060217EQS106M>
- Vollum RJ, Newman JB (1999) Strut and tie models for analysis/design of external beam–column joints. *Mag Concr Res* 51:415–425
- Yurdakul Ö, Del Vecchio C, Di Ludovico M et al (2021a) Crack width-based fragility curves for repairability of substandard beam–column joints. *Bull Earthq Eng* 19:6081–6111
- Yurdakul Ö, Duran B, Tunaboyu O, Avşar Ö (2021b) Field reconnaissance on seismic performance of RC buildings after the January 24, 2020 Elazığ-Sivrice earthquake. *Nat Hazards* 105:859–887

**Publisher's Note** Springer Nature remains neutral with regard to jurisdictional claims in published maps and institutional affiliations.